Ore Geology Reviews 71 (2015) 248–262

Contents lists available at ScienceDirect

Ore Geology Reviews

journal homepage: www.elsevier.com/locate/oregeorev

Some new data on the genesis of the Linghou Cu–Pb–Zn polymetallic deposit—Based on the study of fluid inclusions and C–H–O–S–Pb isotopes

Tang Yanwen [a,*], Li Xiaofeng [a,b], Zhang Xiaoqi [c], Yang Jianling [c], Xie Yuling [d], Lantingguang [a], Huang Youfu [c], Huang Cheng [a], Yin Rongchao [c]

[a] State Key Laboratory of Ore Deposit Geochemistry, Institute of Geochemistry, Chinese Academy of Sciences, Guiyang 550081, China
[b] Key Laboratory of Mineral Resources, Institute of Geology and Geophysics, Chinese Academy of Sciences, Beijing 100029, China
[c] Hangzhou Jiantong Group Co., Ltd., Jiande 311608, China
[d] School of Civil and Environmental Engineering, University of Science and Technology Beijing, Beijing 100083, China

ARTICLE INFO

Article history:
Received 17 November 2014
Received in revised form 5 June 2015
Accepted 7 June 2015
Available online 10 June 2015

Keywords:
Linghou (Jiande) polymetallic deposit
Qinzhou-Hangzhou metallogenic belt
C–H–O–S–Pb isotopes
Fluid immiscibility
Skarn-carbonate replacement type deposit
Ore genesis

ABSTRACT

The Linghou deposit, located near Hangzhou City of Zhejiang Province, eastern China, is a medium-sized polymetallic sulfide deposit associated with granitic intrusion. This deposit is structurally and lithologically controlled and commonly characterized by ore veins or irregular ore lenses. In this deposit, two mineralization events were identified, of which the former produced the Cu–Au–Ag orebodies, while the latter formed Pb–Zn–Cu orebodies. Silicification and calc-silicate (skarn type), phyllic, and carbonate alternation are four principal types of hydrothermal alteration. The early Cu–Au–Ag and late Pb–Zn–Cu mineralizations are characterized by quartz ± sericite + pyrite + chalcopyrite + bornite ± Au–Ag minerals ± magnetite ± molybdenite and calcite + dolomite + sphalerite + pyrite + chalcopyrite + galena, respectively. Calcite clusters and calcite ± quartz vein are formed during the late hydrothermal stage.

The NaCl–H_2O–CO_2 system fluid, coexisting with NaCl–H_2O system fluid and showing the similar homogenization temperatures (385 °C and 356 °C, respectively) and different salinities (16.89–21.68 wt.% NaCl eqv. and 7.70–15.53 wt.% NaCl eqv.), suggests that fluid immiscibility occurred during the Cu–Au–Ag mineralization stage and might have given rise to the ore-metal precipitation. The ore-forming fluid of the Pb–Zn–Cu mineralization mainly belongs to the NaCl–H_2O–CO_2 system of high temperature (~401 °C) and mid-high salinity (10.79 wt.% NaCl eqv.).

Fluids trapped in the quartz-chalcopyrite vein, Cu–Au–Ag ores, Pb–Zn–Cu ores and calcite clusters yielded $\delta^{18}O_{H2O}$ and δD values varying from 5.54‰ to 13.11‰ and from −71.8‰ to −105.1‰, respectively, indicating that magmatic fluids may have played an important role in two mineralization events. The $\delta^{13}C_{PDB}$ values of the calcite change from −2.78‰ to −4.63‰, indicating that the CO_3^{2-} or CO_2 in the ore-forming fluid of the Pb–Zn–Cu mineralization was mainly sourced from the magmatic system, although dissolution of minor marine carbonate may have also occurred during the ore-forming processes. The sulfide minerals have homogeneous lead isotopic compositions with $^{206}Pb/^{204}Pb$ ranging from 17.958 to 18.587, $^{207}Pb/^{204}Pb$ ranging from 15.549 to 15.701, and $^{208}Pb/^{204}Pb$ ranging from 37.976 to 39.052, indicating that metallic elements of the Linghou deposit came from a mixed source involving mantle and crustal components.

Based on geological evidence, fluid inclusions, and H–O–C–S–Pb isotopic data, the Linghou polymetallic deposit is interpreted as a high-temperature, skarn-carbonate replacement type. Two types of mineralization are both related to the magmatic–hydrothermal system, with the Cu–Au–Ag mineralization having a close relationship with granodiorite.

1. Introduction

The Linghou copper–lead–zinc polymetallic deposit, previously named Jiande copper deposit, is an important medium-sized deposit near Hangzhou City of Zhejiang Province, eastern China. This deposit was divided into the Linghou and Songkengwu ore fields. The Linghou ore field contained the Cu–Au–Ag orebodies and was exhausted after forty years of mining. Fortunately, new Cu–Au–Ag and Pb–Zn–Cu orebodies have been found in the Songkengwu ore field since 2003 (Zhen, 2003; Yu, 2010). Previous studies by Chengdu College of Geology and Jiantong Group Co., Ltd. between the 1980s and 2000s were focused on the Cu–Au–Ag orebodies in the Linghou ore field and were instrumental for the understanding of this deposit. However, due to lack of reliable geological and geochemical evidence, the classification of

* Corresponding author at: Institute of Geochemistry, Chinese Academy of Sciences, Guiyang 550081, China.
E-mail address: tyw_xt@126.com (Y. Tang).

http://dx.doi.org/10.1016/j.oregeorev.2015.06.005
0169-1368/

different mineralization events and the genesis of the polymetallic deposit are still debated (Xu et al., 1981; Cao et al., 1988; Zhou et al., 1983; Wang, 1990; Liu et al., 1996). The aim of this paper is to present new field observations of two types of orebodies, fluid inclusions, S–C–O–H–Pb isotope data to identify the different mineralization events, to interpret the sources of the ore-forming fluids and materials, and to provide a better insight into understanding the role of the ore fluid, metallogenic mechanism and ore genesis of the Linghou polymetallic deposit.

2. Geological setting

The Linghou polymetallic deposit is located in the eastern Qinzhou-Hangzhou metallogenic belt (QHMB) between the Yangtze and Cathaysian Blocks (Fig. 1). Several large or super-large deposits, most of which are associated with intrusive rocks, have been found in the eastern QHMB, including famous Dexing porphyry Cu–Mo–Au, Jinshan Au and Yinshan Pb–Zn–Cu polymetallic deposits (Mao et al., 2011a,b; Wang et al., 2011, 2012, 2013; Li et al., 2011, 2012; Zhou et al., 2013a; Guo et al., 2012), Xianglushan skarn W deposit (Zhang et al., 2008; Chen and Zhou, 2012), Dahutang porphyry W deposit (Feng et al., 2012; Mao et al., 2013a), Yongping porphyry Cu–Mo deposit (Li et al., 2013), and Zhangshiba Pb–Zn deposit (Lu et al., 2005). Since 2008, several promising occurrences have been found in this belt in NW Zhejiang, such as Tongcun porphyry Mo–Cu deposit (Qiu et al., 2013; Zeng et al., 2013), Yinshan Pb–Zn–Ag polymetallic deposit (He et al., 2011; Zhou et al., 2013b), and Anji skarn-porphyry Fe–Pb–Zn polymetallic deposit (Xie et al., 2012). As a typical metallogenic belt in eastern China, QHMB was studied during recent years (Mao et al., 2011a,b, 2013b).

The QHMB was interpreted to have resulted from the collision between the Yangtze and Cathaysian Blocks during the Cryogenian (~825 Ma) period (Wang, 1982; Shu, 2006; Yang et al., 2009). However, this belt was reactivated several times during the Caledonian and Yanshanian deformations (Yang and Mei, 1997; Li, 2000; He et al., 2005). Mesozoic tectonomagmatism was related to the collision between the Indochina and Eurasian plates as well as the interaction between the Eurasian and Paleo-Pacific plates (Shu and Zhou, 2002; Wu et al., 2003; Zhou et al., 2006; Yang et al., 2009; Mao et al., 2009; Zheng et al., 2013). The relevant lithosphere extension and thinning provide convenience for asthenospheric upwelling and give rise to intensive intracontinental tectonic and magmatic activities and metallogenesis in eastern China (Wang et al., 2004; Hua et al., 2005; Seton and Müller, 2008; Mao et al., 2009; Xiao et al., 2010; Zhang et al., 2013). The NNE and NE trending faults in eastern QHMB controlled the Yanshanian magmatic activities and the mineralization events (Yang and Mei, 1997; Yang et al., 2009).

3. Geology of the Linghou polymetallic deposit

3.1. Deposit geology

Strata in the Linghou area are made up of Upper Devonian and Middle to Upper Carboniferous sedimentary rocks (BGMRZP, 1989), with the general strike of NE–SW. From older to the younger, the strata are divided into the Upper Devonian Xihu and Zhuzangwu Formations and the Upper Carboniferous Huanglong Formation. The Xihu Formation, 120–130 m thick, is only exposed in two limbs of the Songkengwu syncline (Fig. 2) and mainly consists of the quartz sandstone. The Zhuzangwu Formation is found in the two limbs of the Songkengwu syncline as well as the axis of the Tongshan anticline (Fig. 2), which is estimated to be 64–142 m thick and mainly consists of sandstone-bearing shale and fine sandstone. The Upper and Lower Huanglong Formation is mainly exposed in the axis part of the Songkengwu syncline and composed by the pure limestone (~185 m thick) and limy dolomite (30–35 m thick), respectively. Notably, parts of the stratigraphic successions have been altered and metamorphosed. The carbonate rocks, including marble and dolomite, control the Cu–Au–Ag and Pb–Zn–Cu mineralization.

The structures in the study region are mainly products of the Mesozoic Indosinian and Yanshanian orogenies. The early Indosinian orogeny gave rise to the Songkengwu syncline, Tongshan anticline, and some

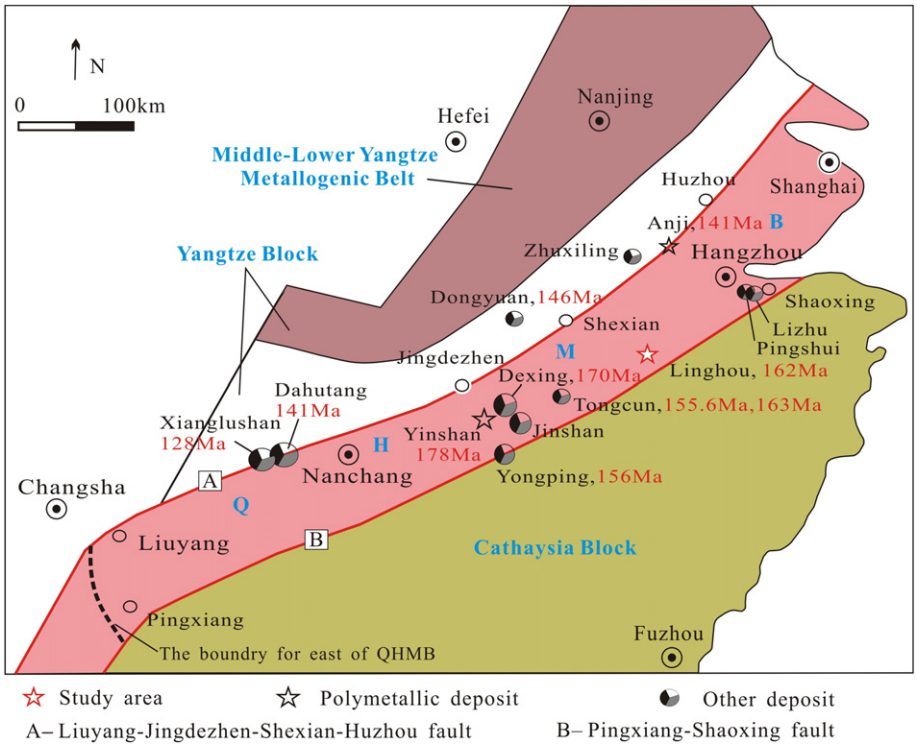

Fig. 1. Spatial-temporal distribution of Mesozoic ore deposits in the east of the Qinzhou-Hangzhou metallogenic belt, eastern China (modified after Yang and Mei, 1997; Mao et al., 2011a, 2013b).

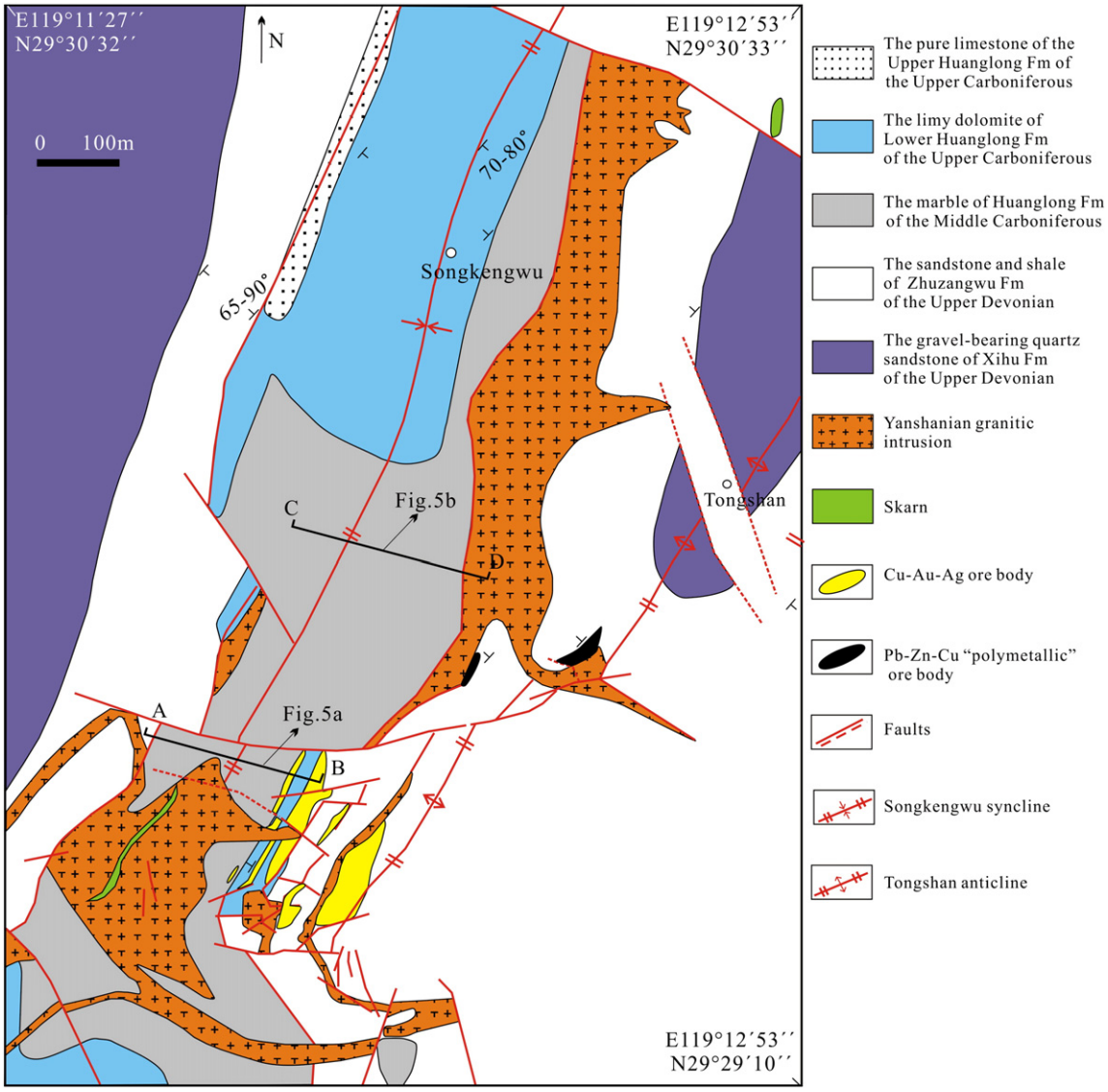

Fig. 2. Geological sketch map of the Linghou polymetallic deposit (modified after Chen, 2005).

coeval faults, whereas the late Yanshanian orogeny commonly reactivated the early structures. Therefore, in the Songkengwu ore field, the principal structures include the Songkengwu syncline and several NE–SW, NW–SE and EW trending faults. Some of them were used by Yanshannian granitic intrusions and the orebodies (Fig. 2).

Previous studies considered that there are multi-stage intrusions in Linghou area (Xu et al., 1981; Zhou et al., 1983; Yu, 2010), although those intrusive rocks are difficult to be identified due to the strong alteration. There is a consensus that granodiorites and granites, especially the former, are principal intrusion controlling the mineralization in the Linghou mine (Xu et al., 1981; Zhou et al., 1983; Yu, 2010; Chen et al., 2013; Jia et al., 2014). In the Songkengwu ore field, the intrusive rocks occupy an axis of the syncline and strike NE–SW (Fig. 2).

3.2. Alteration

The wallrock alteration in chronological order is calc-silicate (skarn) and phyllic alteration, silicification and carbonate alternation in the Linghou mining area. Typical calc-silicate (skarn) alteration was only found at two places in the Songkengwu ore field (Fig. 2). Phyllic alteration is well developed in granitic rocks. It is characterized by disseminated sericite and quartz, with minor pyrite and chalcopyrite. Silicification is closely related to the Cu–Au–Ag mineralization. It is characterized by the quartz in ores (Fig. 3a–e) or quartz + pyrite + chalcopyrite veins in strata and granitic rocks. Carbonate alternation is very common in the mining area. It is characterized by early recrystallization of dolomite + calcite associated with the Pb–Zn–Cu mineralization (Cal-1, Fig. 4c and d), or by late calcite clusters in a hydrothermal calcite cave near the Pb–Zn–Cu orebodies (Fig. 5) and the late calcite (±galena) veins or veinlets (Cal-2) across the ore and granitic rocks (Figs. 3f, 4c and d).

3.3. Ore bodies, ore types and mineralogy

In the Linghou deposit, two different mineralization events were identified, namely the early Cu–Au–Ag (Figs. 2, 5aI) and late Pb–Zn–Cu mineralization. Actually, the Pb–Zn–Cu mineralization is commonly superimposed on the early Cu–Au–Ag mineralization (Fig. 6), forming the Pb–Zn–Cu "polymetallic" orebodies (Figs. 2, 5bII). Both types of orebodies are commonly controlled by the structures and lithologies. They are characterized by ore veins or irregular ore lenses with sharp boundaries against the wall rocks. They show close spatial relationship with the intrusive rocks (Figs. 2, 5).

Cu–Au–Ag orebodies are situated in the southeastern limb of the Songkengwu anticline (Figs. 2, 5a). Among them, the No.I Cu–Au–Ag orebody, enclosed within the Lower Huanglong and Upper Zhuzangwu

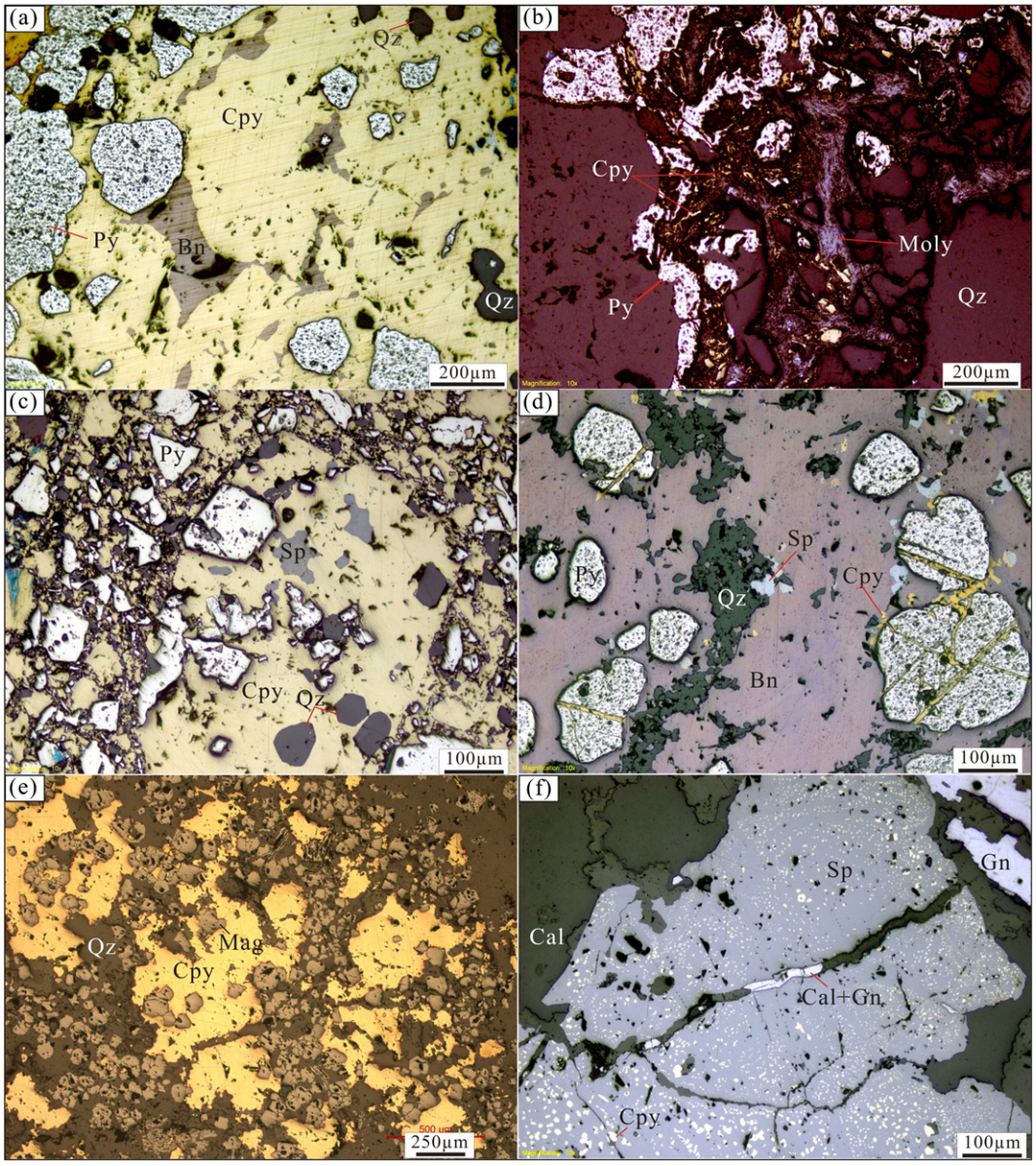

Fig. 3. Mineralogy of two types of orebodies in the Songkengwu ore field. (a) In massive Cu–Au–Ag ores, chalcopyrite coexists with pyrite, bornite and quartz; (b) chalcopyrite + pyrite + molybdenite + quartz vein and veinlet in host rock; (c–d) in massive Cu–Au–Ag ores, chalcopyrite coexists with pyrite, bornite, sphalerite and quartz, but pyrite is earlier than other minerals (reflected light); (e) chalcopyrite + magnetite + quartz vein in hornfels; (f) in Pb–Zn–Cu ore, sphalerite coexists with galena, chalcopyrite, calcite and dolomite, and was intercepted by the late calcite-galena vein (reflected light). Py—pyrite, Cpy—chalcopyrite, Sp—sphalerite, Gn—galena, Bn—bornite, Mag—magnetite, Cal—calcite, Qz—quartz, Moly—molybdenite.

Formations (Fig. 5a), was traced for 81 m downdip, 135 m along strike and 1.7–12.0 m across, with the general strike of 16° NNE and dip of 57°–72°. This orebody contains 2.9 thousand tons of Cu at a grade of 1.80 wt.%, 5.9 kg of Au at a grade of 0.12 g/t and 3.56 t of Ag at a grade of 22.41 g/t (Chen, 2005). The primary ores are mainly massive and banded. Ore minerals are composed by dominant chalcopyrite and bornite, with minor pyrite, gold, silver minerals (found only in chalcopyrite), sphalerite, magnetite, molybdenite, or by abundant pyrite and minor chalcopyrite. Gangue minerals are quartz, minor calcite and dolomite (Figs. 3a–e, 4a and b). The sulfide minerals are mainly massive and banded, forming veins within the host rock, with rare veinlet-disseminated structures.

The Pb–Zn–Cu "polymetallic" orebodies occur in the center of the Songkengwu anticline (Figs. 2, 5b). The No.II Pb–Zn–Cu "polymetallic" orebody was traced for 168 m downdip, 170 m along strike, and is 2.3–35.1 m across, with the trend to NW and the dip of 40°–65°. This ore body contains 33.0 thousand tons of Cu at a grade of 3.71 wt.%, 31.9 thousand tons of Zn at a grade of 3.58 wt.%, 0.5 t Au at a grade of 0.58 g/t and 68.25 t of Ag at a grade of 76.74 g/t (Chen, 2005). The massive and banded ores are composed by sphalerite, chalcopyrite, pyrite and galena, with calcite and dolomite as gangue minerals (Figs. 3f, 4c and d). The sulfide minerals form mainly massive, banded and vein bodies within the host rock.

3.4. Mineralization stages

In this study, we mainly focus on the Songkengwu ore field to interpret the mineralization stages and mineralogical assemblages of the Linghou polymetallic deposit. On the basis of mineralogical assemblages and cross-cutting relationships of different veins (Figs. 3f, 4 and 6), the mineralization stages can be described as follows: (1) the early calc-silicate (skarn) alteration stage, as reported by Zhou et al. (1983) and Xu et al. (1981), is characterized by the mineralogical assemblage of wollastonite + garnet + diopside + serpentine + chlorite ± epidote;

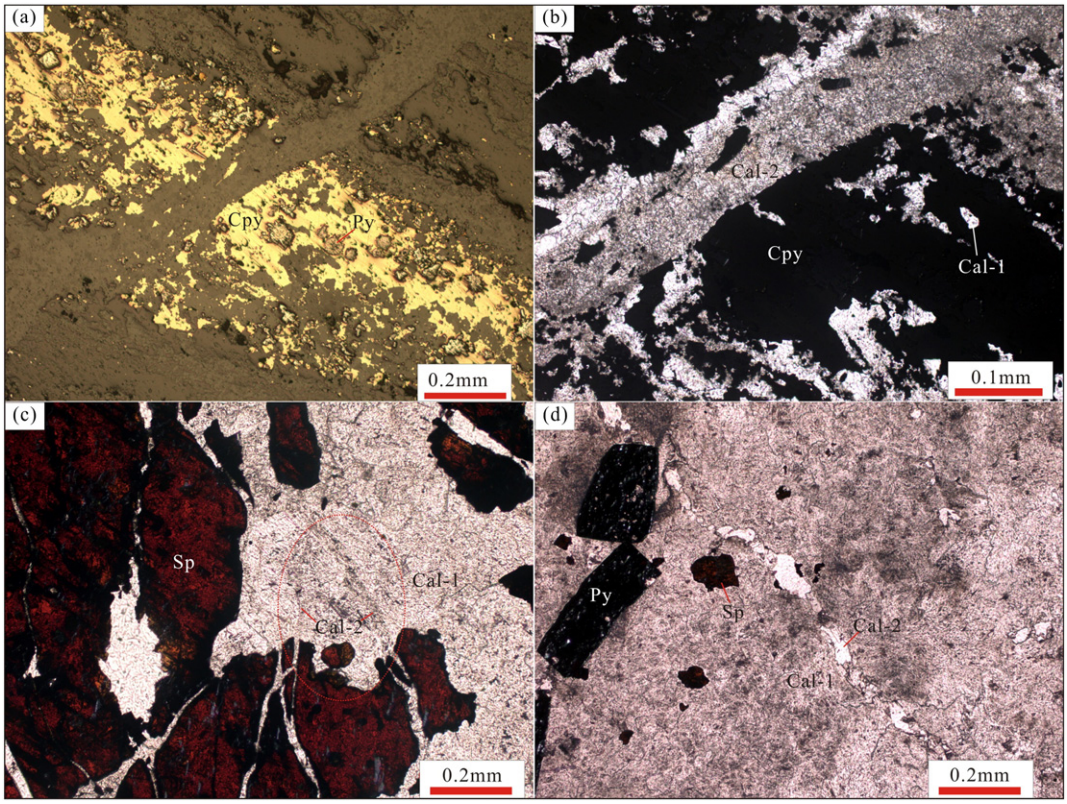

Fig. 4. The relationship between two types of mineralization and the late calcite vein. (a–b) The late calcite vein cross-cut the chalcopyrite + pyrite vein in reflected (a) and polarized (b) light; (c–d) the late calcite vein (Cal-2) cross-cut the sphalerite and coeval calcite + dolomite (Cal-1) off (polarized light).

(2) the Cu–Au–Ag mineralization stage is characterized by the mineralogical assemblage of quartz ± sericite + pyrite + chalcopyrite + bornite + Au–Ag minerals ± magnetite ± molybdenite; (3) the Pb–Zn–Cu mineralization stage is represented by calcite + dolomite + sphalerite + pyrite + chalcopyrite + galena; and (4) post mineralization stage produced calcite clusters in the hydrothermal calcite cave and calcite ± quartz veins with the width ranging from 1 to 4 mm. The mineralization stages and paragenetic sequences are shown in Fig. 7.

4. Samples and analytical methods

The samples, including altered and mineralized granitoids near the orebodies, quartz-sulfides veins, Pb–Zn–Cu ores and calcite clusters, are used for detailed petrographic study of the fluid inclusions. The samples are listed in Table 1. Microthermometric measurements were carried out at the State Key Laboratory of Ore Deposit Geochemistry, Institute of Geochemistry, Chinese Academy of Sciences, Guiyang, China. Fluid inclusions microthermometry data were obtained from quartz and calcite on a Linkam THMSG-600 heating-freezing stage, coupled with a Zeiss microscope. The stage enables measurements within the range of −196 and 600 °C. For freezing runs, the precision is about ±0.1 °C for ice melting; for heating runs, and the precision is about ±0.5 °C for critical point. The compositions of single fluid inclusion were measured by Renishaw inVia Reflex Raman microprobe by an argon ion laser with a laser source of 514 nm in the State Key Laboratory of Ore Deposit Geochemistry, Institute of Geochemistry, Chinese Academy of Sciences. The scanning range of spectra was set between 100 and 4300 cm^{-1} with an accumulation time of 60 s for each scan; the laser beam width is about 1 μm, and spectral resolution is about 0.14 cm^{-1}.

Eight samples of quartz, pyrite and calcite were selected for H–O isotope analyses. The H–O isotopic compositions were measured by a MAT253 mass spectrometer in the Geological Analysis Laboratory under the Ministry of Nuclear Industry, Beijing, China. Oxygen was liberated from quartz by reaction with BrF_5. Isotopic data were reported in per mil relative to the Vienna SMOW standard for oxygen and hydrogen. Total uncertainties were estimated to be better than ±0.2‰ for $\delta^{18}O$ and ±2.0‰ for δD at the 1σ level.

Sulfur isotopic analyses are performed on pyrite, chalcopyrite, bornite, sphalerite and galena from Cu–Au–Ag and Pb–Zn–Cu ores. Sulfur isotope analyses were carried out at the State Key Laboratory of Environmental Geochemistry, Institute of Geochemistry, Chinese Academy of Sciences, using a continuous flow mass spectrometer. GBW04415 and GBW04414 Ag_2S were used as the external standards, and the relative errors (2σ) were better than 0.1‰. Sulfur isotopic compositions are reported to CDT.

Two samples from the Pb–Zn ores, one sample from the late calcite vein in Pb–Zn ores, and two samples from calcite clusters in the hydrothermal calcite cave near the Pb–Zn–Cu ores were selected for C–O isotope analyses. The C–O isotopic compositions were obtained using a MAT-251 EM mass spectrometer at the State Key Laboratory of Environmental Geochemistry, Institute of Geochemistry, Chinese Academy of Sciences. Calcite reacts with pure phosphoric acid to produce CO_2. The analytical precisions (2σ) are ±0.2‰ for carbon isotopes and ±2‰ for oxygen isotopes. The C–O isotopic compositions are reported to PDB. The value of $\delta^{18}O_{SMOW}$ is calculated by $\delta^{18}O_{SMOW} = 1.03086 \times \delta^{18}O_{PDB} + 30.86$ (Friedman and O'Neil, 1977).

Lead isotopic compositions were analyzed using the IsoProbe-T thermal ionization mass spectrometer (TIMS) at the Geological Analysis Laboratory under the Ministry of Nuclear Industry, Beijing, China. Lead was separated and purified by using a conventional cation-exchange technique and taking diluted HBr as eluant. Lead isotopic ratios of all samples were reported relative to the measured ratio for NBS981 standard material. The precision of the $^{208}Pb/^{206}Pb$ measurement (1 μg of Pb) is ≤0.005%, and the measured ratios (2σ) of international standard sample NBS981 are $^{208}Pb/^{204}Pb = 36.611 \pm 0.004$, $^{207}Pb/^{204}Pb = 15.457 \pm 0.002$, and

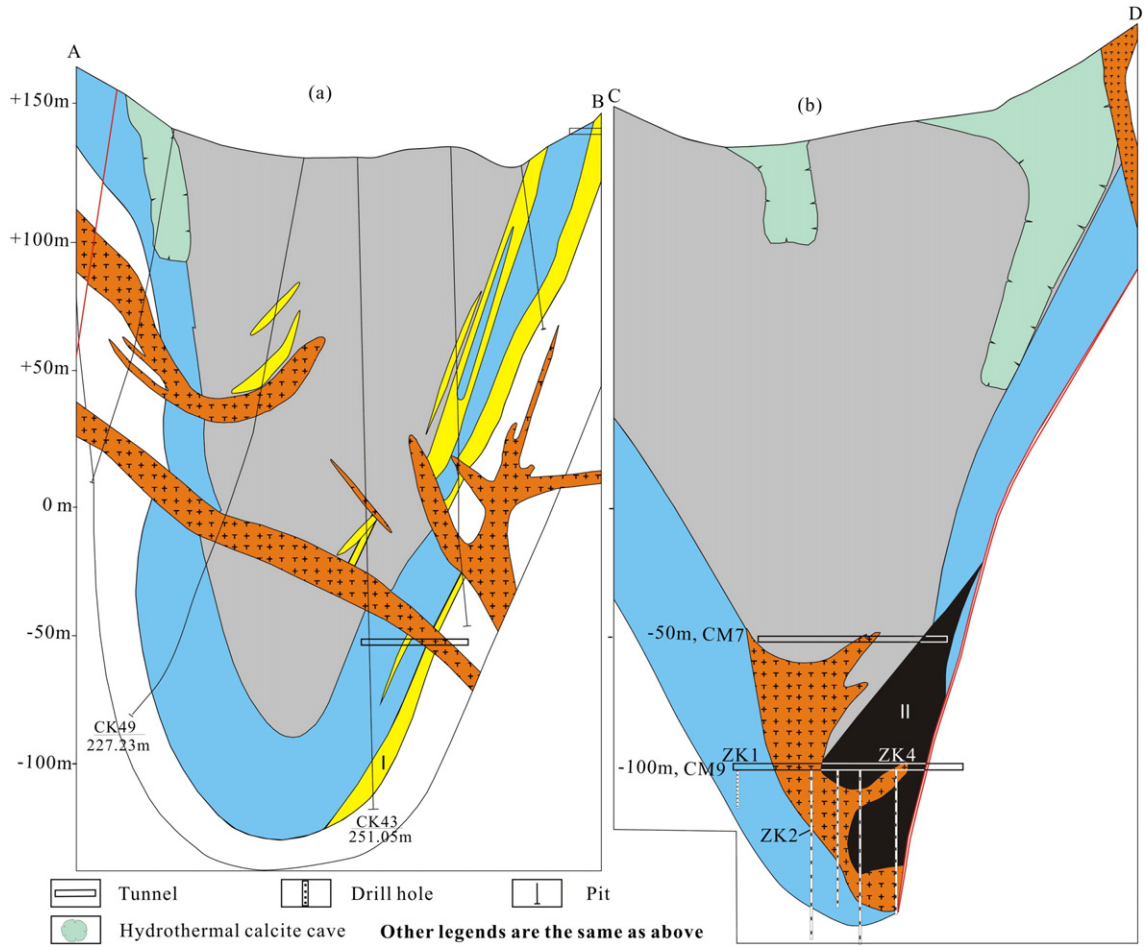

Fig. 5. Geological cross-section of exploration lines A–B and C–D (see in Fig. 2 for location) of the Linghou deposit (modified after Yu, 2010; Chen, 2005).

$^{206}Pb/^{204}Pb = 16.937 \pm 0.002$, in agreement with the reference value (Belshaw et al., 1998).

5. Results

5.1. Fluid inclusions

5.1.1. Petrography of fluid inclusions

Abundant fluid inclusions are observed at room temperature (<20 °C) (Fig. 8). The primary fluid inclusions are distributed in isolation or as a group. They vary dramatically in shape, including rounded, oval, triangular and irregular, with the general size of 15 × 10 μm and the largest size of 20 × 18 μm.

On the basis of their composition and phases, three types of fluid inclusions were identified:

The C-type-CO_2-bearing two-phase (vapor CO_2 + liquid H_2O) inclusions are common in quartz phenocrysts from the mineralized granitoids, in calcite from the Pb–Zn ores and also in the quartz + chalcopyrite veins. They usually have ellipsoidal, irregular or negative crystal shapes with the size ranging from 15 to 22 μm. Relatively smaller sizes of 9–13 μm are observed in the quartz + pyrite ± chalcopyrite veins in the granitoids. The CO_2 phase often occupies 40–60% in volume and is homogenized to liquid.

The H-type-aqueous two-phase (vapor H_2O + liquid H_2O) inclusions are hosted mainly in the quartz-sulfide veins and in the calcite clusters. This type of fluid inclusions consists of gas and liquid aqueous salt solutions, and is homogenized to liquid after heating. The vapor phase of H-type fluid inclusions, especially in the calcite clusters, is usually <20% in volume (Fig. 8d–f).

The A-type-aqueous liquid phase fluid inclusions are only found in coexistence with H-type fluid inclusions in calcite clusters and commonly show irregular shapes (Fig. 8f).

Based on petrographic observations, both C- and H-type fluid inclusions were dominant during the Cu–Au–Ag mineralization stage, whereas dominant C-type and minor H-type fluid inclusions were typical during the Pb–Zn–Cu mineralization stage. All types of fluid inclusions are found in late calcite clusters.

5.1.2. Microthermometry

The microthermometric data are summarized in Table 1. Salinity was calculated using the data of Bodnar (1993) and Hall et al. (1988), and density was calculated using T–W-ρ phase diagram from Bodnar (1983).

Fifty-seven C-type fluid inclusions from the Cu–Au–Ag mineralization were analyzed, which show the clathrate melting temperature of 0–5.8 °C (with an average value of 2.4 °C) and the homogenization temperature of 300–470 °C (averaging 385 °C). The corresponding salinities of those fluid inclusions are from 7.70 to 15.53 wt.% NaCl eqv. (averaging 12.58 wt.% NaCl eqv.). Another twenty-three H-type fluid inclusions give the ice melting temperature of −13.0 to −19.0 °C (averaging −16.0 °C) and the homogenization temperature of 305–417 °C (with an average value of 356 °C). The corresponding salinities of the fluid inclusions are from 16.89 to 21.68 wt.% NaCl eqv. (averaging 19.39 wt.% NaCl eqv.), and all the densities range between 0.77 and 0.90 g/cm^3 (averaging 0.85 g/cm^3).

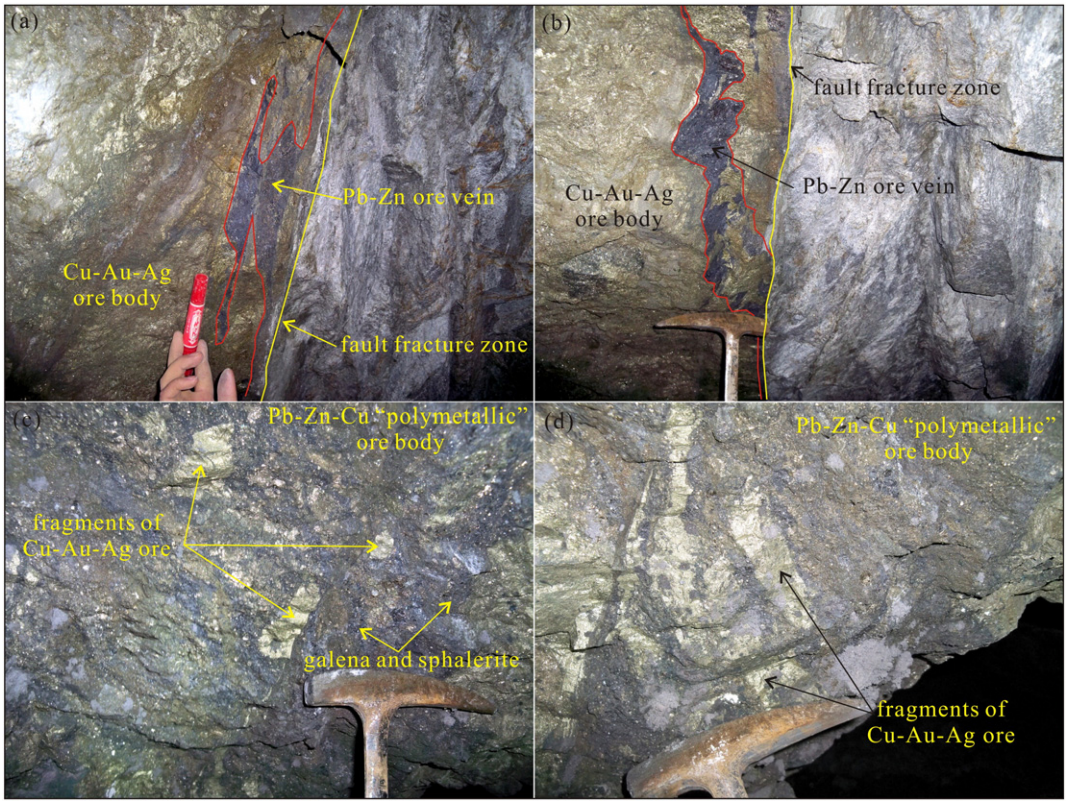

Fig. 6. Geological evidence for two mineralization events in the Linghou Cu–Pb–Zn polymetallic deposit. (a–b) The late black Pb–Zn ore veins occurred along the fault and cross-cut the early Cu–Au–Ag ore body; (c–d) the late Pb–Zn ore body overprinted the early Cu–Au–Ag ore body and entrapped the fragments of Cu–Au–Ag ore, producing the Pb–Zn–Cu "polymetallic" ore body.

Seventeen C-type fluid inclusions of the Pb–Zn–Cu mineralization were analyzed. The melting temperature of clathrate is 2.5–5.2 °C (mean 3.7 °C), and the homogenization temperatures range from 350 to 480 °C, with a mean of 401 °C. The corresponding salinities vary from 8.66 to 12.55 wt.% NaCl eqv. (mean 10.79.% NaCl eqv.). One H-type fluid inclusion gives an ice-melting and homogenization temperature of −5.5 °C and 450 °C, with the corresponding salinity of 19.3 wt.% NaCl eqv. and the density of 0.47 g/cm^3, respectively.

For the late calcite clusters near the Pb–Zn orebodies, fourteen H-type fluid inclusions were analyzed. The melting temperature of ice is

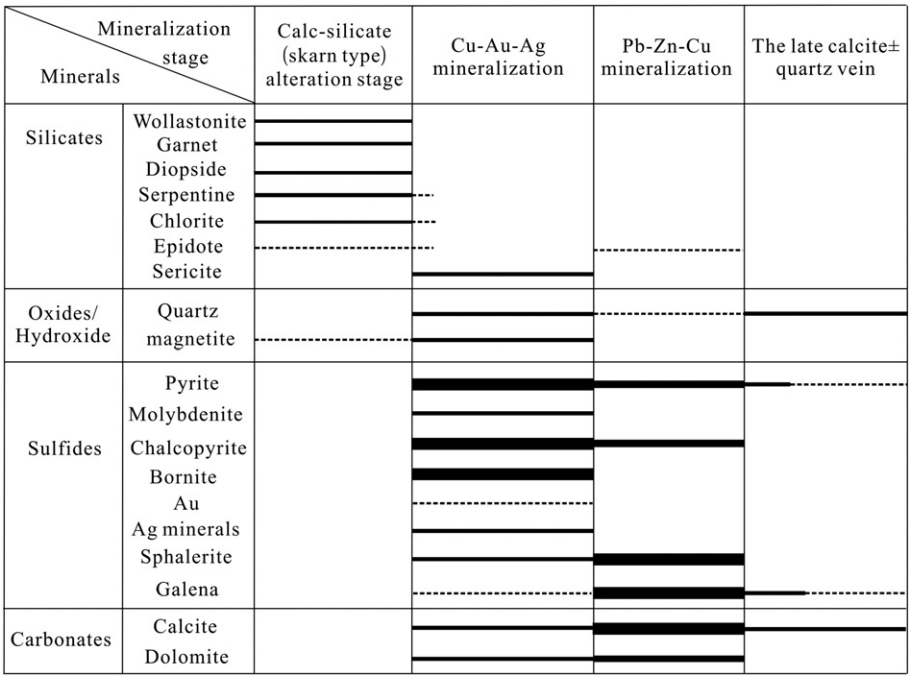

Fig. 7. Mineralization stages and paragenetic sequences for the Linghou polymetallic deposit.

Table 1
Microthermometric results of primary fluid inclusions in the Linghou polymetallic deposit.

Sample no.	Mineral	Lithology	Type	Number	$Tm_{clath/ice}$ (°C)	Th (°C) (average)	Salinity (wt.% $NaCl_{eqv}$)	Density (g/cm^3)	P/10^5 Pa
The Cu–Au–Ag mineralization stage									
JDB059	Quartz	Cu mineralization granitoid	C	7	0.4–1.4(1.0)	390–420(411)	13.69–15.09(14.35)		
JDB059	Quartz		H	3	−15–16.5(−15.7)	410–417(414)	18.63–19.84(19.17)	0.77–0.79(0.78)	
JDB015	Quartz	Qz–Py–Cpy vein in granitoid	C	9	1.9–5.8(3.4)	330–470(404)	7.7–13.32(8.73)		
JDB017	Quartz	Qz–Py–Cpy vein in granitoid	C	12	2.6–4.5(3.5)	300–412(368)	9.74–12.42(11.25)		
JDB007	Quartz	Qz–Py vein in granitoid	C	6	2.5–3.6(2.9)	300–400(364)	11.05–12.55(12.28)		
JDB007	Quartz		H	7	−13–18(−14.6)	315–370(351)	16.89–20.97(18.24)	0.82–0.90(0.85)	101–190(153)
JDB050	Quartz	Mo–Cpy–Py vein	H	13	−13.2–19.0(16.9)	305–393(346)	16.99–21.68(20.06)	0.81–0.93(0.87)	80–237(148)
JDB050	Quartz		C	23	0–3.9(2.0)	300–420(378)	10.62–15.53(13.15)		
Average						385			
The Pb–Zn–Cu mineralization stage									
JDB022	Calcite	Pb–Zn ore	C	17	2.5–5.2(3.7)	350–480(401)	8.66–12.55(10.79)		
JDB022	Calcite		H	1	−5.5	450	19.3	0.47	430
Average						405			
The late quartz-calcite stage									
JDB003	Calcite	Calcite clusters	C	6	0.3–1.5(0.8)		13.82–15.2(14.69)		
JDB003	Calcite		H	14	−4–8.4(−6.3)	180–203(191)	6.45–12.16(10.36)	0.93–0.98(0.96)	8–13(10.8)

$Tm_{clath/ice}$: temperature of clathrate or ice melting; Th_{CO2}: homogenization temperature of the CO_2 phase; Th: homogenization temperature of vapor H_2O or CO_2 to liquid H_2O.

−4.0 to −8.4 °C (averaging −6.3 °C), and the homogenization temperatures range from 180 to 203 °C, with a mean of 191 °C. The corresponding salinities vary from 6.45 to 12.16 wt.% NaCl eqv. (averaging 10.36 wt.% NaCl eqv.), and the densities are 0.93–0.98 g/cm^3 (averaging 0.96 g/cm^3). Another six C-type fluid inclusions were analyzed, showing the clathrate melting temperatures of 0.3–1.5 °C (averaging 0.8 °C), and the corresponding salinities of 13.82–15.2 wt.% NaCl eqv. (averaging 14.69% NaCl eqv.).

The histograms of homogenization temperatures of all types of fluid inclusions and the relationships between the homogenization temperatures and the salinities are shown in Figs. 9 and 10.

5.1.3. Laser Raman spectroscopy

The gas phase components of the C- and H-type fluid inclusions are analyzed by the laser Raman spectroscope. The representative results are shown in Fig. 11. The vapor phase of the C-type fluid inclusions mainly contains CO_2 (1386.51 cm^{-1}) and H_2O (3381.58 cm^{-1}) (Fig. 11a). The vapor phase of the H-type fluid inclusions is mainly H_2O (3384, 3420 cm^{-1}) (Fig. 11b).

Unfortunately, the gas phase of the C- and H-types fluid inclusions in calcite cannot be tested due to the high background values.

5.2. H–O isotopic compositions

The H–O isotopic compositions are shown in Table 2 and Fig. 12. The $\delta^{18}O$ value of fluid was calculated using the average homogenization temperature of the fluid inclusions from each mineral (Table 1). The mineral–water fractionation factors of oxygen isotope are from Clayton et al. (1972) (quartz-water: $1000\ln a = 3.38 * 10^6/T^2 - 3.40$) and O'Neil et al. (1969) (calcite-water: $1000\ln a = 2.78 * 10^6/T^2 - 3.40$). As a result, the quartz and pyrite from the Cu–Au–Ag ores show the $\delta^{18}O_{H2O}$ values ranging from 9.23‰ to 12.77‰, and the corresponding δD values of fluid vary from −74.9‰ to −105.1‰. The calcite and pyrite from the Pb–Zn ores have the $\delta^{18}O_{H2O}$ values of 7.5‰ and 11.76‰, and the corresponding δD values are −104.1‰ and −82.7‰, respectively. Three late calcites give $\delta^{18}O_{H2O}$ and δD values, ranging from 5.54‰ to 13.11‰ and from −71.8‰ to −88.9‰, respectively.

5.3. Carbon and oxygen isotopes

The $\delta^{13}C$ and $\delta^{18}O$ values of five calcite samples are listed in Table 3 and plotted in Fig. 13. Two early calcite samples from the Pb–Zn ores give $\delta^{13}C$ values of −3.38‰ to −2.78‰ and $\delta^{18}O$ values of 13.40‰–14.40‰. The $\delta^{13}C$ and $\delta^{18}O$ values of three late calcite samples fall within a narrow range of −3.97‰ to −4.64‰ and 15.04‰–16.09‰, respectively.

5.4. Sulfur isotope systematics

Sulfur isotopic compositions of sulfide minerals are listed in Table 4 and plotted in Fig. 14. All samples from the Cu–Au–Ag ores are characterized by the low and positive $\delta^{34}S$ values, ranging from +1.76‰ to +4.30‰, with an average value of +2.90‰. For the samples from Pb–Zn–Cu ores, the $\delta^{34}S$ values range from −1.42‰ to +2.25‰, with a mean of +0.93‰.

5.5. Lead isotopes

Lead isotopic compositions of sulfides from the Cu–Au–Ag and Pb–Zn–Cu ores are listed in Table 5 and plotted in Fig. 15. The sulfides have homogeneous radiogenic lead isotopic compositions, showing $^{206}Pb/^{204}Pb$ ranging from 17.958 to 18.587, $^{207}Pb/^{204}Pb$ ranging from 15.549 to 15.701, and $^{208}Pb/^{204}Pb$ ranging from 37.976 to 39.052, respectively.

6. Discussion

6.1. Sources of ore-forming fluids and materials

6.1.1. Ore-forming fluids

The $\delta^{18}O_{H2O}$ and δD_{H2O} values of the fluids from two mineralization stages plot near the magmatic water field (Fig. 12), which suggests that magmatic fluids may have played an important role during the formation of the ore-forming fluids. However, compared with the typical magmatic water, the δD values of the fluids in this study are significantly lower (Fig. 12). As previous studies (Rye, 1993) proposed, we attribute such isotopic changes to degassing of magma chamber. Two samples of the late calcite plot in the left of the magmatic fluid box, indicating that some meteoric water were probably incorporated in late calcite ± quartz stage.

The $\delta^{13}C$ values of calcite samples from the Pb–Zn ores and the late calcite samples give the $\delta^{13}C$ values of −4.64‰ to −2.78‰, higher than those of the organic matter (averaging −25‰, Hoefs, 2009), atmospheric CO_2 (about −8‰, Schidlowski, 1998 or −7‰ to −11‰, Hoefs, 1997), CO_2 dissolved in water (−9‰ to −20‰, Hoefs, 1997), crust (−7‰, Faure, 1986) and mantle (−5‰ to −7‰, Hoefs, 2009), and lower than the marine carbonates (~0‰, Hoefs, 2009), but fall in the range of igneous/magma systems (−3‰ to −30‰, Hoefs, 1997). Actually, on the $\delta^{18}O$ vs. $\delta^{13}C$ diagram, the samples mainly plot within or

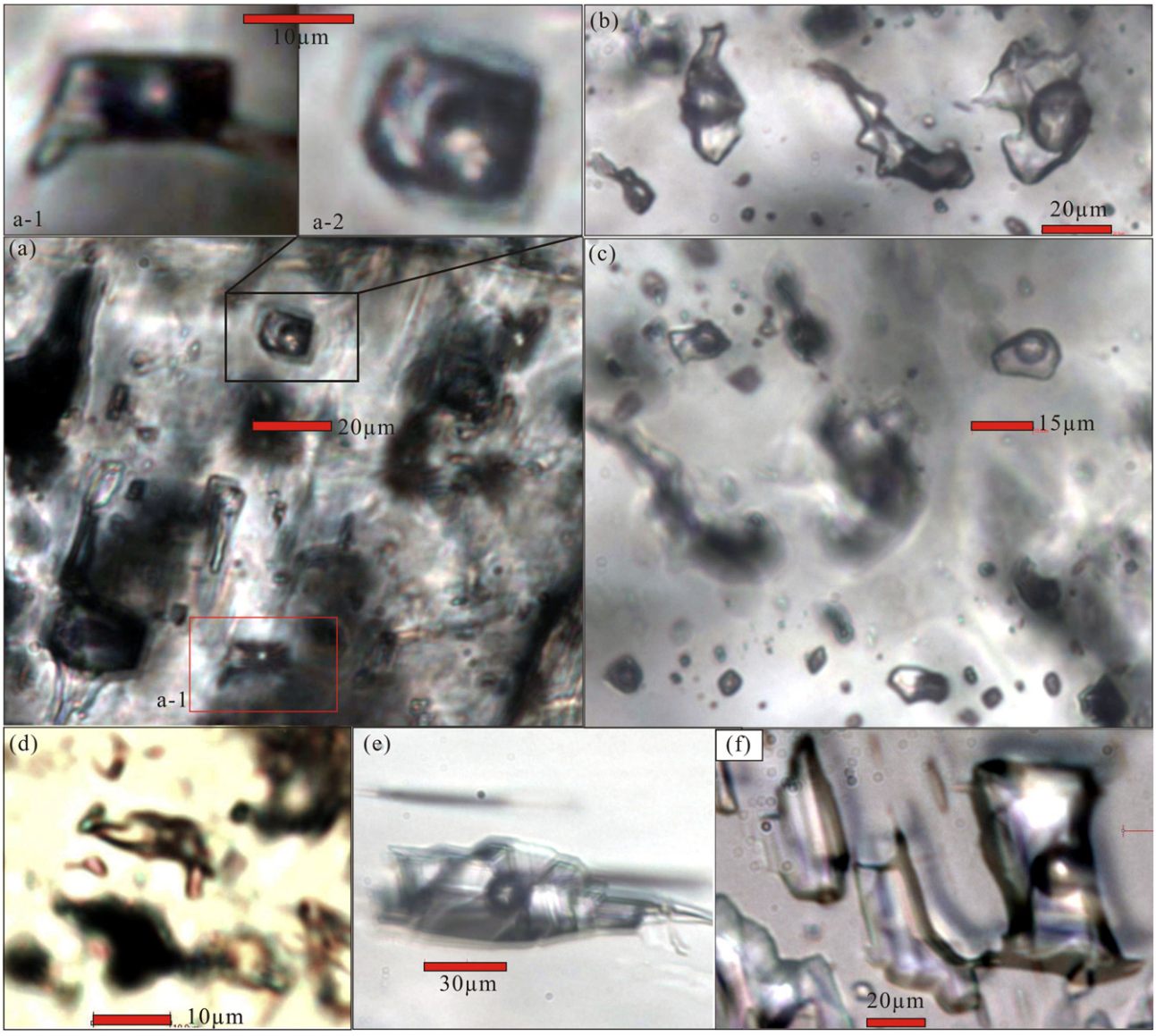

Fig. 8. The types and characteristics of fluid inclusions in the Linghou deposit. (a) The primary C-type fluid inclusions in the calcite of the Pb–Zn ore; (b) the primary C-type fluid inclusions with the irregular shape in the quartz + chalcopyrite + pyrite + molybdenite vein; (c) the primary C-type fluid inclusions in the quartz + chalcopyrite + pyrite + molybdenite vein; (d) H-type fluid inclusions in the quartz + pyrite + chalcopyrite + molybdenite veins; (e–f) H-type fluid inclusions in calcite clusters; (f) A-type fluid inclusions coexists with H-type fluid inclusions in calcite clusters.

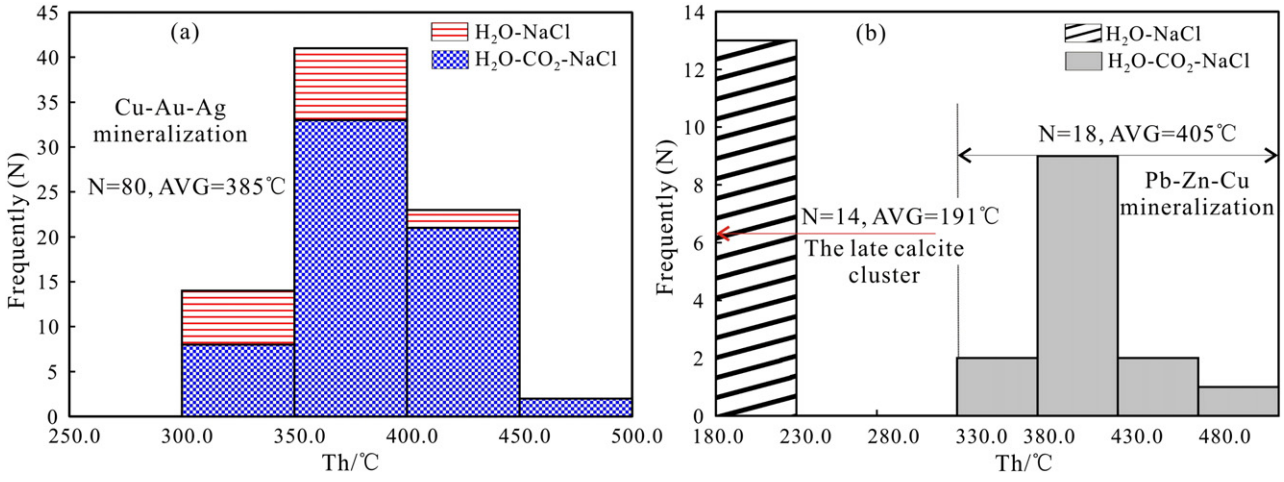

Fig. 9. Histograms of homogenization temperatures measured for fluid inclusions of different hydrothermal stages.

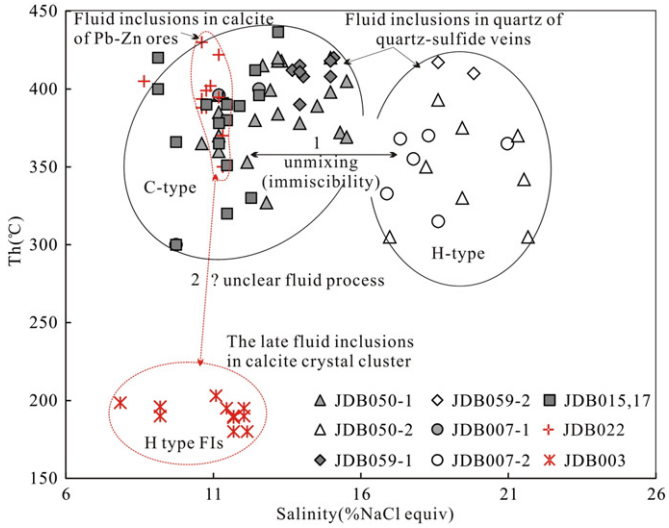

Fig. 10. Relationships between homogenization temperatures and salinities of fluid inclusions in the Linghou polymetallic deposit.

near the granite box field (Fig. 13), indicating that the CO_3^{2-} or CO_2 in the ore-forming fluids were mainly sourced from magmatic system. Notably, the samples also show obvious trend of low-temperature alteration or contamination by marine carbonate (Fig. 13). Considering that most orebodies of the deposit hosted in the carbonate rocks of the Huanglong Formation (Fig. 5), we regard that dissolution of the marine carbonate may contribute to the ore-forming fluids.

6.1.2. Ore-forming materials

The $\delta^{34}S$ values of sulfides from the Cu–Au–Ag and Pb–Zn–Cu ores have a narrow range of −1.42‰ to +4.30‰, which correspond to the magmatic systems (−3‰ to +7‰, Ohmoto and Goldhaber, 1997). This indicates that the sources of sulfur in the Linghou deposit were most likely derived from the magmatic sulfur.

All the sulfides have homogeneous lead isotopic compositions, and most of them plot near the orogenic Pb evolution curve of Zartman and Doe (1981) (Fig. 15). This indicates that metals of ores in the Linghou deposit came from a mixed source of mantle and crust.

6.2. Evidence of two mineralization events

In this paper, we propose that there were two mineralization events in the Linghou polymetallic deposit, namely the early Cu–Au–Ag and late Pb–Zn–Cu mineralizations. Three principal facts support this: 1) *Geologically*, the late black Pb–Zn–Cu ore veins intercept the early Cu–Au–Ag orebody (Fig. 6a and b) and several fragments of copper ore were trapped in the Pb–Zn–Cu orebody (Fig. 6c and d); 2) *Different mineralogical assemblages* in the early Cu–Au–Ag and late Pb–Zn–Cu mineralization are characterized by quartz + chalcopyrite ± pyrite ± bornite + sphalerite ± Au–Ag minerals and calcite + dolomite + sphalerite + galena + chalcopyrite + pyrite, respectively; and 3) *Different types of fluid inclusions* of the early Cu–Au–Ag mineralization are represented by CO_2-dearing two-phase fluid inclusions and aqueous two-phase fluid inclusions, but fluid inclusions in the Pb–Zn–Cu ore are dominated by the CO_2-dearing two-phase type. The homogenization temperature of the late Pb–Zn–Cu mineralization is a little higher than the fluid inclusions from the early Cu–Au–Ag ore (veins) (Table 1).

Table 2
Oxygen and hydrogen isotopic data for fluid in quartz, calcite and pyrite from the Songkengwu orefield.

Sample no.	Mineral	$\delta^{18}O_{V-SMOW}$/‰	$\delta^{18}O_{H2O}$/‰	δD_{H2O}/‰	T_h (°C)	Description of samples
JDB007	Quartz	17.7	12.77	−74.9	364	Qz–Py–Cpy vein in
JDB015	Quartz	13.2	9.23	−85.1	404	granitoid
JDB026-1	Pyrite		10.1	−105.1		Massive Cu–Au–Ag ore
JDB005	Pyrite		7.5	−104.2		Pb–Zn–Cu ore
JDB022	Calcite	14.40	11.76	−82.7	405	Pb–Zn–Cu ore
JDB045	Calcite	16.09	13.11	−88.9	191	Calcite vein in Pb–Zn–Cu ore
JDB031	Calcite	15.04	5.54	−72.1	191	Calcite clusters in
JDB038	Calcite	15.72	6.22	−71.8	191	cave

Th: homogenization temperature.

6.3. Possible fluid processes and metallogenic mechanism for the Cu–Au–Ag mineralization

C-type fluid inclusions coexist with H-type fluid inclusions in quartz from the quartz–sulfide veins (Table 1; Fig. 8) and show similar homogenization temperatures (385 °C and 356 °C, respectively) and different salinities (Fig. 10, 7.70–15.53 wt.% NaCl eqv. and 16.89–21.68 wt.% NaCl eqv., respectively). These characteristics are consistent with fluid immiscibility (Fan et al., 2006; Wang et al., 2015), indicating that path 1 on Fig. 10 represents a fluid immiscibility process during the Cu–Au–Ag mineralization stage. Of course, fluid immiscibility process has been described in many other skarn deposit, e.g., Bismark Pb–Zn–Cu–Ag (Baker and Lang, 2003), Vegas Peladas Fe (Pons and Franchini, 2009), Kensu

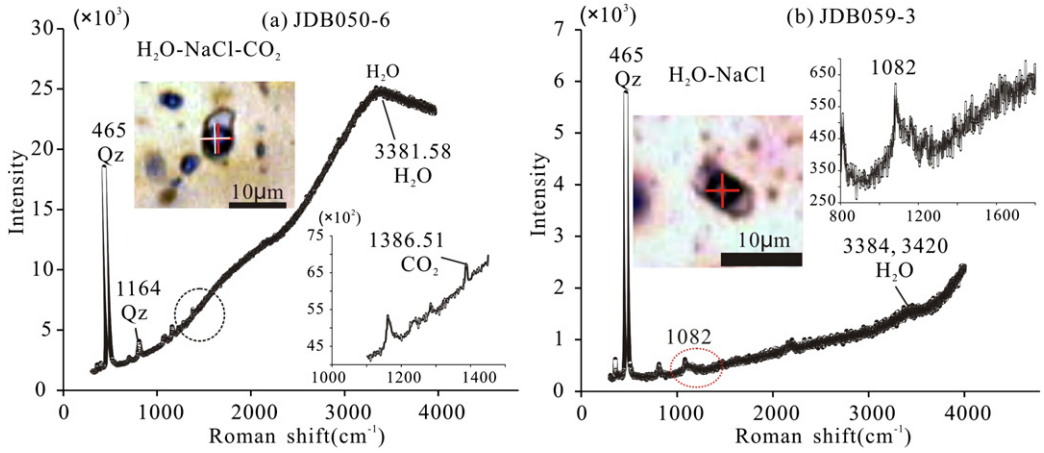

Fig. 11. Representative Raman spectra of fluid inclusions in the Linghou polymetallic deposit. (a) H_2O- and CO_2-spectrum of vapor phase in C-type fluid inclusion; (b) H_2O-spectrum of vapor phase in H-type fluid inclusion.

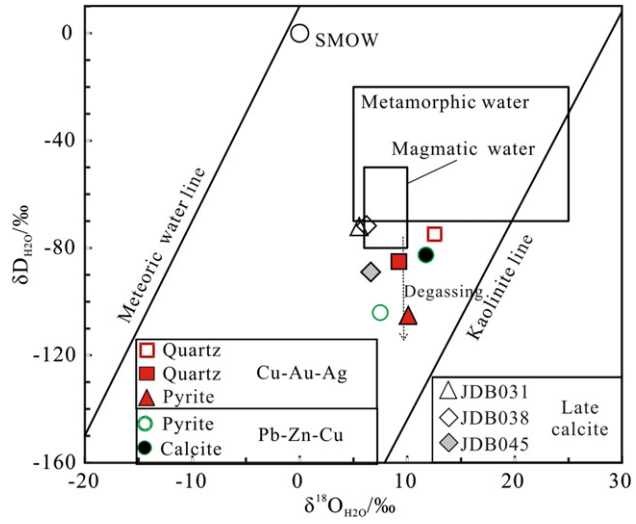

Fig. 12. δD_{H2O} (‰)–$\delta^{18}O_{H2O}$(‰) plots of the Cu–Au–Ag and Pb–Zn–Cu mineralization and the late calcite in the Linghou polymetallic deposit.

Table 3
Oxygen and carbon isotopic compositions of calcite located in or near the Pb–Zn–Cu orebodies.

Sample no.	Object	$\delta^{13}C_{PDB}$/‰	$\delta^{18}O_{SMOW}$/‰	Description of samples
JDB005	Calcite	−2.78	13.40	The Pb–Zn ore
JDB022	Calcite	−3.38	14.40	The Pb–Zn ore
JDB045	Calcite	−4.64	16.09	Late calcite vein in Pb–Zn ore
JDB031	Calcite	−4.23	15.04	Calcite clusters in cave
JDB038	Calcite	−3.97	15.72	Calcite clusters in cave

W–Mo (Soloviev, 2011) and Baiyinnuo'er Zn–Pb deposits (Shu et al., 2013). Generally, during the ascending of granitic magma, the progressive decompression or crystallization-induced degassing will give rise to different fluid systems with variable salinities and densities (Lowenstern, 2001; Heinrich, 2005; Yang and Scott, 2006), such as a low salinity and density, CO_2-rich and H_2O-poor vapor system and a high-density, saline liquid system (Schandl and Wicks, 1993; Yang and Scott, 2002, 2006; Heinrich, 2005; Chi et al., 2006; Wysoczanski et al., 2012). Considering the ore-controlling conditions in the Linghou deposit, similar with other skarn deposits (Baker and Lang, 2003; Soloviev, 2011), decompression (e.g., from lithostatic pressure to hydrostatic pressure) is considered to cause the fluid immiscibility (not including boiling). It has been thought to be an important mechanism of mineralization in copper–gold (Fu et al., 2003), REE–Nb–Fe (Fan et al., 2006), and gold deposits (Lu, 2011; Wang et al., 2015). Therefore, this process might also be responsible for the ore deposition during the Cu–Au–Ag mineralization stage to some extent.

6.4. Ore genesis

Combining the relationships between the orebodies and the granodiorite porphyry, as well as the characteristics of alteration and mineralization, some researchers classified this deposit as a skarn-type associated with magmatic–hydrothermal systems (Xu et al., 1981; Zhou et al., 1983). Besides the magmatic contribution, Wang (1990) also stressed that this deposit was controlled by the host rocks and structure. However, based on the shapes of the bedded orebodies, Cao et al. (1988) and Liu et al. (1996) considered that this deposit was a SEDEX-type and was overprinted by late magmatic–hydrothermal activities. Although the formation of skarn may produce a very characteristic alteration pattern, it is not universally developed in the Linghou mining area, and most of the orebodies were hosted in the carbonate rocks. Those characteristics are similar to the typical skarn-carbonate replacement type deposit, such as the carbonate-hosted Ag–Pb–Zn (Cu) deposit of northern Mexico (Megaw et al., 1988), the Uchucchacua Ag–Mn–Pb–Zn (Bussell et al., 1990), the Janggun Pb–Zn–Ag (Koo et al., 2000), Homestake Au–Cu–Ag (Johnson and Thompson, 2006) and the Lavrion Pb–Zn–Ag deposits (Bonsall et al., 2011). Therefore, the Linghou polymetallic deposit can be interpreted as a skarn-carbonate replacement type. The spatial distribution of alteration, Cu–Au–Ag orebodies and granodiorite indicate a close relationship between the Cu–Au–Ag mineralization and the granodiorite. Nonetheless, further studies on mineralization age are still required in order to identify the relationships between the Pb–Zn–Cu mineralization and the different units of the granitoids.

7. Conclusions

Two mineralization events formed two types of orebodies in the Linghou polymetallic deposit, including the early Cu–Au–Ag and late Pb–Zn–Cu mineralizations. The first mineralization is characterized by mineralogical assemblages of quartz + chalcopyrite + pyrite +

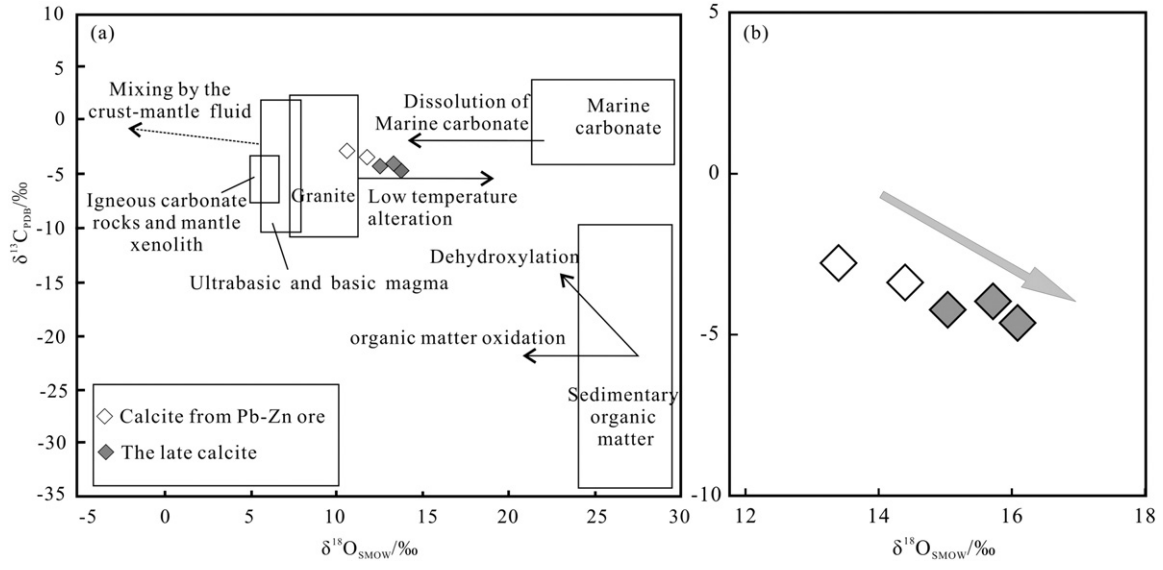

Fig. 13. Plots of $\delta^{13}C_{PDB}$ versus $\delta^{18}O_{SMOW}$ for the calcite in the Linghou polymetallic deposit (modified after Liu and Liu, 1997; Mao et al., 2002).

Table 4
Sulfur isotopic data of sulfides from two different types of mineralization in the Linghou deposit.

Sample	Mineral	$\delta^{34}S‰$	Location	Geology of sample	Source
The early Cu–Au–Ag mineralization					
	Pyrite	4.30	CD505I	Breccia Cu–Py ore	Liu et al., 1996
	Pyrite	1.78	CD505I	Breccia Cu–Py ore	
	Pyrite	1.76	CD2II	Massive Cu–Py ore	
	Pyrite	2.58	CD505II	Massive Cu–Py ore	
JDB023	Pyrite	2.80	NO.2 stope, −150 m	Massive Cu ore	This paper
JDB026	Chalcopyrite	3.80	NO.1 stope, −150 m	Massive Cu ore	This paper
JDB023	Bornite	3.30	NO.2 stope, −150 m	Massive Cu ore	This paper
Average value		**2.90**			
Pb–Zn–Cu mineralization					
JDB011	Pyrite	1.6	Pb–Zn–Cu orebody in No.29 exploration line	Pb–Zn–Cu ore	This paper
	Chalcopyrite	2.16	CD3II	The banded Pb–Zn–Cu ore	Liu et al., 1996
	Sphalerite	1.19	The west of NO.2 transverse drift at −50 m south of mining area	Pb–Zn–Cu ore	
	Sphalerite	1.19	ZK47-4	Pb–Zn ore	
	Sphalerite	2.25	Pb–Zn–Cu ore body	Pb–Zn ore	
	Sphalerite	1.67	Pb–Zn–Cu ore body	Pb–Zn ore	
	Sphalerite	0.84	Pb–Zn–Cu ore body	Pb–Zn ore	
	Galena	0.33	Pb–Zn–Cu ore body	Pb–Zn ore	
	Galena	−1.42	The west of NO.2 transverse drift at −50 m south of mining area,	Pb–Zn ore	
	Galena	−0.48	ZK47-4	Pb–Zn ore	
Average value		**0.93**			

bornite + Au–Ag minerals ± magnetite ± molybdenite, whereas the latter is featured by calcite + dolomite + shpalerite + galena + chalcopyrite + pyrite.

Petrographic observations, microthermometry data and Laser Raman spectroscopy analysis show that the fluid inclusions of the early Cu–Au–Ag mineralization are represented by NaCl–H_2O and NaCl–H_2O–CO_2 systems, both of which show high temperature and high salinity. In contrast, the fluids of the Pb–Zn–Cu mineralization mainly belong to the NaCl–H_2O–CO_2 system and also show high temperature and mid-high salinity. Fluid immiscibility occurred in Cu–Au–Ag mineralization stage and might be responsible for the ore deposition.

The H–O isotope systematics suggest that magmatic fluids played an important role in the ore-forming processes of the Linghou polymetallic deposit. Notably, for the Pb–Zn–Cu mineralization, meteoric water was probably incorporated into the late calcite ± quartz stage. The $\delta^{13}C$ values of the calcite suggest that the CO_3^{2-} or CO_2 in the ore-forming fluid of the Pb–Zn–Cu mineralization was mainly sourced from magmatic system, but the dissolution of marine carbonate may have also been involved in. The $\delta^{34}S$ values of sulfides from the Cu–Au–Ag and Pb–Zn–Cu ores are similar to those of the magmatic systems, indicating that the sulfur in the Linghou deposit was sourced from magmatic sulfur. Lead isotopic compositions show that metallic elements of the ores came from a mixed source involving the mantle and the crust.

The geological evidence, fluid inclusion, and H–O–C–S–Pb isotopic data indicate that the Linghou polymetallic deposit exhibits the characteristics of high-temperature, skarn-carbonate replacement type deposit, and two types of mineralization in this deposit are both related to the magmatic–hydrothermal systems. The Cu–Au–Ag mineralization has an especially close relationship with the granodiorite.

Conflict of interest

The authors declared that they have no conflicts of interest to this work.

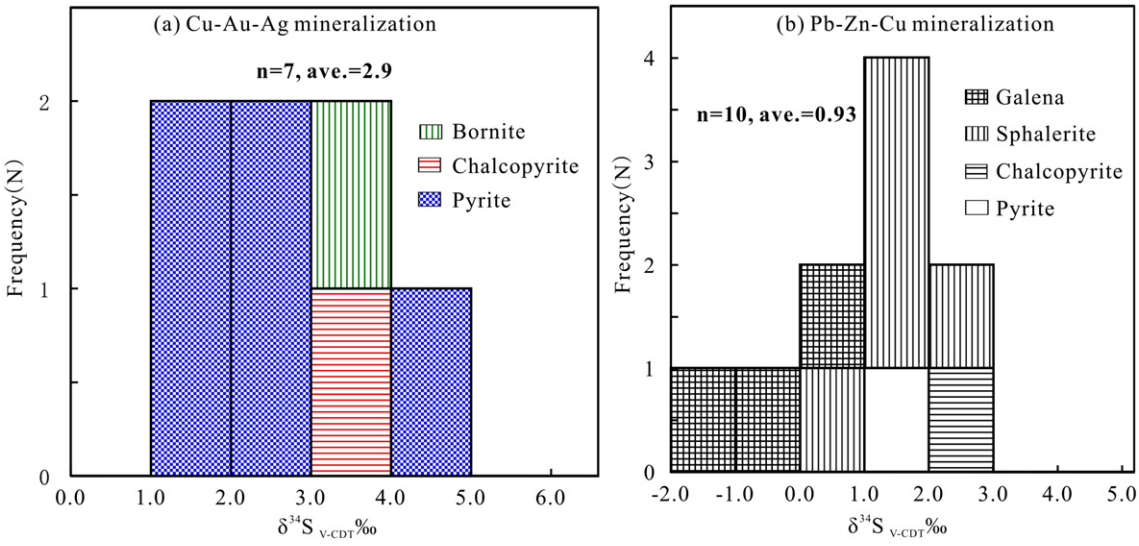

Fig. 14. Histograms of $\delta^{34}S$ values of sulfide minerals from the Cu–Au–Ag and Pb–Zn–Cu orebodies in the Linghou polymetallic deposit.

Table 5
Lead isotopic compositions of the sulfides from the Linghou polymetallic district.

Sample	Minerals	$^{206}Pb/^{204}Pb$	$^{207}Pb/^{204}Pb$	$^{208}Pb/^{204}Pb$	Location	Reference
Cu–Au–Ag mineralization						
LJD-1	Py	18.148	15.580	38.120	Cu–Au–Ag ore	Liu et al., 1996
Pb–Zn–Cu mineralization						
JDB005	Sp	18.044	15.569	38.172	NO.2 stope, −50 m	This paper
JDB011	Cpy	18.587	15.701	39.052	Pb–Zn–Cu orebody in No.29 exploration line	
JDB011	Sp	18.453	15.606	38.638		
LJD-2	Gn	18.091	15.653	38.341	Pb–Zn–Cu orebody	Liu et al., 1996
LJD-3	Py	18.130	15.588	38.054	Pb–Zn–Cu orebody	
LJD-4	Gn	17.971	15.560	38.072	Pb–Zn–Cu orebody	
LJD-5	Gn	18.001	15.549	37.976	Pb–Zn–Cu orebody	Liu et al., 1996
LJD-6	Gn	18.110	15.661	38.331	Pb–Zn–Cu orebody	
LJD-7	Gn	18.078	15.627	38.190	Pb–Zn–Cu orebody	
LJD-8	Gn	18.077	15.583	38.279	Pb–Zn–Cu orebody	
LJD-9	Gn	17.958	15.573	38.116	Pb–Zn–Cu orebody	
Average (n = 10)		**18.136**	**15.606**	**38.293**		

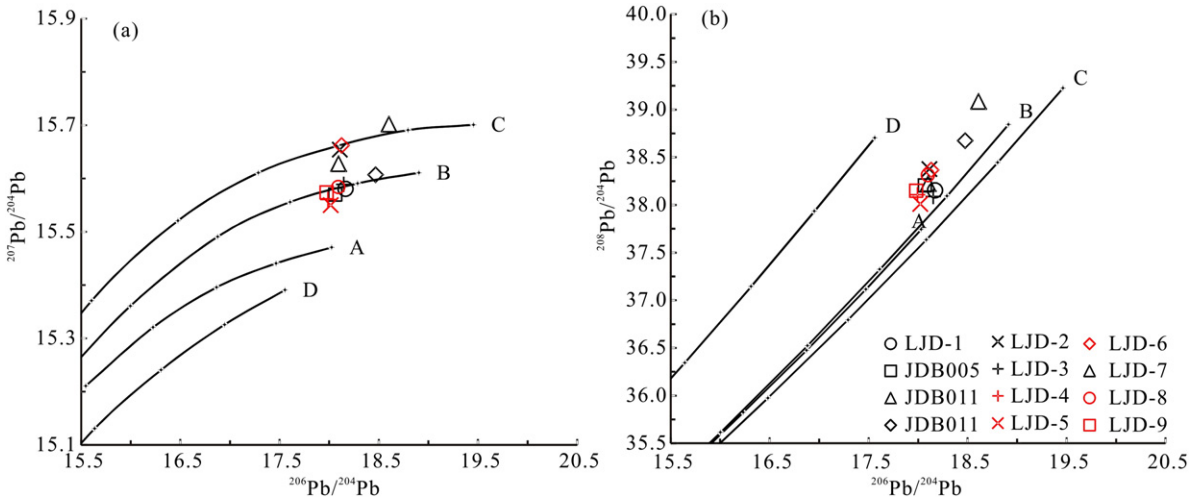

Fig. 15. Plots of $^{207}Pb/^{204}Pb$ vs. $^{206}Pb/^{204}Pb$ and $^{208}Pb/^{204}Pb$ vs. $^{206}Pb/^{204}Pb$ for the sulfides of the Linghou polymetallic deposit. A—Mantle; B—orogen; C—upper crust; D—lower crust.

Acknowledgments

This study was financially supported by the State Key Fundamental Research Project of China (2012CB416705), the 12th Five-Year Plan project of the National Science & Technology Pillar Program (2011BAB04B02), the Frontier Program (Y3CJ001000) from the Institute of Geochemistry, Chinese Academy of Sciences, and the Frontier Program (Y3KJA20001) from the State Key Laboratory of Ore Deposit Geochemistry. We are also grateful to Dr. Franco Pirajno, Editor-in-Chief, Dr. Alexander Yakubchuk, Associate Editor, and Dr. Konstantin Lobanov for their thorough, helpful, and constructive comments.

References

Baker, T., Lang, J.R., 2003. Reconciling fluid inclusion types, fluid processes, and fluid sources in skarns: an example from the Bismark Deposit, Mexico. Mineral. Deposita 38, 474–495.

Belshaw, N.S., Freedman, P.A., O'Nions, R.K., Frank, M., Guo, Y., 1998. A new variable dispersion double-focusing plasma mass spectrometer with performance illustrated for Pb isotopes. Int. J. Mass Spectrom. 181, 51–58.

BGMRZP (Bureau of Geology and Mineral Resources of Zhejiang Province), 1989. Regional geology of Zhejiang Province. People's Republic of China. Ministry of Geology and Mineral Resources. Geol. Mem 11 (1), 85–107. Geological Publishing House; Beijing (In Chinese).

Bodnar, R.J., 1983. A method of calculating fluid inclusion volumes based on vapor bubble diameters and P–V–T–X properties of inclusion fluids. Econ. Geol. 78, 535–542.

Bodnar, R.J., 1993. Revised equation and table for determining the freezing point depression of H_2O–NaCl solutions. Geochim. Cosmochim. Acta 57, 683–684.

Bonsall, T.A., Spry, P.G., Voudouris, P.C., Tombros, S., Seymour, K.S., Melfos, V., 2011. The Lavrion District, Attica, Greece: fluid inclusion, stable isotope, and rare earth element studies. Econ. Geol. 106, 619–651.

Bussell, M.A., Alpers, C.N., Petersen, U., Shepherd, T.J., Bermudez, C., Baxter, A.N., 1990. The Ag–Mn–Pb–Zn vein, replacement, and skarn deposits of Uchucchacua, Peru: studies of structure, mineralogy, metal zoning, sr isotopes, and fluid inclusion. Econ. Geol. 85, 1348–1383.

Cao, S.Y., Liu, J.J., Li, Y.L., 1988. Characteristics and the model of Linghou polymetallic deposit—the marine volcanic-hydrothermal sedimentary type deposit in Zhejiang province. J. Chengdu Inst. Geol. 15, 11–20 (in Chinese).

Chen, B.S., 2005. The geological survey report of Songkengwu ore field (No. 33–30 lines) in Jiande copper deposit, Zhejiang province. Zhejiang Institute of Geology and Mineral Exploration for Non-ferrous Metals, pp. 5–6 (In Chinese).

Chen, B., Zhou, X.X., 2012. Ore-controlling factors and a metallogenic model for the Xianglushan Tungsten-ore field in northern Jiangxi Province. Geol. Explor. 48, 0562–0569 (In Chinese with English abstract).

Chen, L., Wang, Z.Q., Zhao, Y.Y., Liu, Y., Cao, J., Ding, L., Qu, W.J., 2013. Re–Os isotopic dating of pyrrhotite in the Linghou Cu deposit, Jiande, Zhejiang province and its geological significance. Acta Geol. Sin. 87 (12), 1864–1873 (In Chinese with English abstract).

Chi, G.X., Dubé, B., Williamson, K., Williams-Jones, A.E., 2006. Formation of the Campbell-Red Lake gold deposit by H_2O-poor, CO_2-dominated fluids. Mineral. Deposita 40, 726–741.

Clayton, R.N., O'Neil, J.R., Mayeda, T.K., 1972. Oxygen isotope exchange between quartz and water. J. Geophys. Res. 77, 3057–3067.

Fan, H.R., Hu, F.F., Yang, K.F., Wang, K.Y., 2006. Fluid unmixing/immiscibility as an ore-forming process in the giant REE–Nb–Fe deposit, Inner Mongolian, China: evidence from fluid inclusions. J. Geochem. Explor. 89, 104–107.

Faure, G., 1986. Principles of Isotope Geology. Second edition. John Wiley & Sons, New York, p. 589.

Feng, C.Y., Zhang, D.Q., Xiang, X.K., Li, D.X., Qu, H.Y., Liu, J.N., Xiao, Y., 2012. Re–Os isotopic dating of molybdenite from the Dahutang tungsten deposit in northwestern Jiangxi Province and its geological implication. Acta Petrol. Sin. 28 (12), 3858–3868 (In Chinese with English abstract).

Friedman, L., O'Neil, J.R., 1977. Compilation of stable isotope fractionation factors of geochemical interest: data of geochemistry. U. S. Geol. Surv. Prof. Pap. 440-KK.

Fu, B., Williams, P.J., Oliver, N.H.S., Dong, G.Y., Pollard, P.J., Mark, G.M., 2003. Fluid mixing versus unmixing as an ore-forming process in the Cloncurry Fe-oxide–Cu–Au District,

NW Queensland, Australia: evidence from fluid inclusions. J. Geochem. Explor. 78–79, 617–622.
Guo, S., Zhao, Y.Y., Qu, H.C., Wu, D.X., Xu, H., Li, C., Liu, Y., Zhu, X.Y., Wang, Z.K., 2012. Geological characteristics and ore-forming time of the Dexing porphyry copper ore mine in Jiangxi province. Acta Geol. Sin. (Engl. Ed.) 86, 691–899.
Hall, D.L., Sterners, S.M., Bodnar, R.J., 1988. Freezing point depression of NaCl–KCl–H_2O solutions. Econ. Geol. 83, 197–202.
He, J.R., Wang, A.G., Rui, X.J., Li, C.H., 2005. Discussion on mineralizing process in east integrating zone of Qinzhou Bay and Hangzhou Bay: in Earth science technology forum of six provinces and one municipality in East China, 2005. Jiangsu Geological Institute, Nanjing, Jiangsu Province, China, pp. 8–13 (In Chinese with English abstract).
He, G.J., Yang, X.C., Wu, G.M., Zhang, G.F., Cai, X.X., Zheng, J., 2011. A study of ore mineral characteristics and metallogenic stages of the Yinshan Ag–Pb–Zn polymetallic ore deposit, northwest Zhejiang province. Acta Geosci. Sin. 32, 304–312 (In Chinese with English abstract).
Heinrich, C.A., 2005. The physical and chemical evolution of low-salinity magmatic fluids at the porphyry to epithermal transition: a thermodynamic study. Mineral. Deposita 39, 864–889.
Hoefs, J., 1997. Stable Isotope Geochemistry. 3rd edition. Springer-Verlag, Berlin Heidelberg, pp. 1–201.
Hoefs, J., 2009. Stable Isotope Geochemistry. 6th edition. Springer-Verlag, Berlin Heidelberg, pp. 48–54.
Hua, R.M., Chen, P.R., Zhang, W.L., Lu, J.J., 2005. Three major metallogenic events in Mesozoic in South China. Mineral Deposits 11, 291–304 (In Chinese with English abstract).
Jia, S.H., Zhao, Y.Y., Wang, Z.Q., Wu, Y.D., Wang, T., Chen, L., 2014. Zircon U–Pb dating and geochemical characteristics of granodiorite-porphyry in the Linghou copper deposit, Western Zhejiang, and their geological significance. Acta Geol. Sin. 88 (11), 2071–2085 (In Chinese with English abstract).
Johnson, T.W., Thompson, T.B., 2006. Breccia- and carbonate-hosted Au–Cu–Ag replacement mineralization associated with the homestake porphyry intrusive complex, New World District, Montana. Econ. Geol. 101, 955–980.
Koo, L.H., Hee, L.C., Cheal, Y.B., Chang, L.J., 2000. Geology, mineralogy and geochemistry of carbonate replacement-type lead–zinc–silver deposits in Janggun Mine, Republic of Korea. J. China Univ. Geosci. 11, 100–102.
Li, Y.G., 2000. Qiantang–Qingfang old plate junction zone and its geological significance. Geol. Zhejiang 16, 17–24 (In Chinese with English abstract).
Li, X.F., Xiao, R., Feng, Z.H., Wang, C.Y., Yang, F., Bai, Y.P., Jiang, S.K., Wang, Z.K., Zhu, X.Y., Xiao, N., Wei, X.L., 2011. Zircon SHRIMP U–Pb and biotite Ar–Ar ages from Fujiawu porphyry Cu–Mo deposit, Dexing, Southeast China: implications for magmatic–hydrothermal chronology. Let's Talk Ore Deposits Vols. I and II pp. 377–379.
Li, X.F., Hu, R.Z., Wei, X.L., Xiao, R., Xiao, N., Wang, C.Y., Yang, F., 2012. Mineral deposits types, mineralization features and genesis relationship between Jinshan gold deposit and Deixing porphyry copper deposit, northeastern Jiangxi province, South China. Geol. Rev. 58 (1), 82–90 (In Chinese with English abstract).
Li, X.F., Watanabe, Y., Yi, X.K., 2013. Ages and sources of Ore-related porphyries at Yongping Cu–Mo deposit in Jiangxi province, southeast China. Resour. Geol. 63, 288–312.
Liu, J.M., Liu, J.J., 1997. Basinal fluid genetic model of fine disseminated gold deposits in the golden triangle area between Yunnan, Guizhou and Guangxi. Acta Mineral. Sin. 17, 448–456 (In Chinese with English abstract).
Liu, J.J., Cao, S.Y., Li, Y.L., 1996. Origin of the Jiande copper deposit, Zhejiang. Miner. Resour. Geol. 10, 145–154 (In Chinese with English abstract).
Lowenstern, J.B., 2001. Carbon dioxide in magmas and implications for hydrothermal systems. Mineral. Deposita 36, 490–502.
Lu, H.Z., 2011. Fluids immiscibility and fluid inclusions. Acta Petrol. Sin. 27 (5), 1253–1261 (In Chinese with English abstract).
Lu, S.D., Gao, W.L., Wang, S.L., Xiao, E., Xu, J.H., Liu, J., 2005. Pb isotopic compositions and its significance for ore genesis in Zhangshiba Pb–Zn deposit, Jiangxi. J. Mineral. Petrol. 25, 64–69 (In Chinese with English abstract).
Mao, J.W., He, Y., Ding, T.P., 2002. Mantle fluids involved in metallogenesis of Jiaodong (east Shandong) gold district: evidence of C, O and H isotopes. Mineral Deposits 21, 121–127 (In Chinese with English abstract).
Mao, J.R., Yutaka, T., Li, Z.L., Takahashi, N., Ye, H.M., Zhao, X.L., Zhou, J., Hu, Q., Zeng, Q.T., 2009. Correlation of Meso-Cenozoic tectono-magmatism between SE China and Japan. Geol. Bull. China 28, 844–856 (In Chinese with English abstract).
Mao, J.W., Chen, M.H., Yuan, S.D., Guo, C.L., 2011a. Geological characteristics of the Qinhang (or Shihang) Metallogenic Belt in South China and spatial–temporal distribution regularity of mineral deposits. Acta Geol. Sin. 85, 636–658 (In Chinese with English abstract).
Mao, J.W., Zhang, J.D., Pirajno, F., Ishiyama, D., Su, H.M., Guo, C.L., Chen, Y.C., 2011b. Porphyry Cu–Au–Mo-epithermal Ag–Pb–Zn-distal hydrothermal Au deposits in the Dexing area, Jiangxi province, East China—a linked ore system. Ore Geol. Rev. 43, 203–216.
Mao, Z.H., Cheng, Y.B., Liu, J.J., Yuan, S.D., Wu, S.H., Xiang, X.K., Luo, X.H., 2013a. Geology and molybdenite Re–Os age of the Dahutang granite-related veinlets-disseminated tungsten ore field in the Jiangxin Province, China. Ore Geol. Rev. 53, 422–433.
Mao, J.W., Cheng, Y.B., Chen, M.H., Pirajno, F., 2013b. Major types and time–space distribution of Mesozoic ore deposits in South China and their geodynamic settings. Mineral. Deposita 48, 267–294.
Megaw, P.K.M., Ruiz, J., Titley, S.R., 1988. High-temperature, carbonate-hosted Ag–Pb–Zn (Cu) deposits of Northern Mexico. Econ. Geol. 83, 1856–1885.
Ohmoto, H., Goldhaber, M.B., 1997. Sulfur and carbon isotopes. In: Barnes, H.L. (Ed.), Geochemistry of Hydrothermal Ore Deposits, 3rd edition John Wiley and Sons, New York, pp. 517–611.
O'Neil, J.R., Clayton, R.N., Mayeda, T.K., 1969. Oxygen isotope fractionation in divalent metal carbonate. J. Chem. Phys. 51, 5547–5558.
Pons, J.M., Franchini, M., 2009. Iron skarns of the Vegas Peladas District, Mendoza, Argentina. Econ. Geol. 104, 157–184.
Qiu, J.T., Yu, X.Q., Santosh, M., Zhang, D.H., Chen, S.Q., Li, P.J., 2013. Geochronology and magmatic oxygen fugacity of the Tongcun molybdenum deposit, northwest Zhejiang, SE China. Mineral. Deposita 48, 545–556.
Rye, R.O., 1993. The evolution of magmatic fluids in the epithermal environment: the stable isotope perspective. Econ. Geol. 88, 733–753.
Schandl, E.S., Wicks, F.J., 1993. Carbonate and associated alteration of ultramafic and rhyolitic rocks at the Hemingway property, Kidd creek volcanic complex, Timmins, Ontario. Econ. Geol. 88, 1615–1635.
Schidlowski, M., 1998. Beginnings of terrestrial life: problems of the early record and implications for extraterrestrial scenarios. Instrum. Methods Missions Astrobiol. SPIE 3441, 149–157.
Seton, M., Müller, R.D., 2008. Reconstructing the junction between Panthalassa and Tethys since the Early Cretaceous. PESA Eastern Australasian Basins Symposium III, Sydney, 14–17 September, pp. 263–266 (earthbyte.org).
Shu, L.S., 2006. Predevonian tectonic is evolution of South China from Cathaysian block to Caledonian period folded orogenic belt. Geol. J. China Univ. 12, 418–431 (In Chinese with English abstract).
Shu, L.S., Zhou, X.M., 2002. Late Mesozoic tectonism of Southeast China. Geol. Rev. 48 (3), 249–260 (in Chinese with English abstract).
Shu, Q.H., Lai, Y., Sun, Y., Wang, C., Meng, S., 2013. Ore genesis and hydrothermal evolution of the Baiyinnuo'er zinc–lead skarn deposit, Northeast China: evidence from isotopes (S, Pb) and fluid inclusions. Econ. Geol. 108, 835–860.
Soloviev, S., 2011. Geology, mineralization, and fluid inclusion characteristics of the Kensu W–Mo skarn and Mo–W–Cu–Au alkalic porphyry deposit, Tien Shan, Kyrgyzstan. Econ. Geol. 106, 193–222.
Wang, H.C., 1982. The main stages of crustal development of China. Earth Sci. 7, 155–177 (In Chinese with English abstract).
Wang, Z.J., 1990. The exploration model for Jiande copper deposit. Miner. Resour. Geol. East China 11–22 (in Chinese).
Wang, Q., Zhao, Z.H., Jian, P., Xu, J.F., Bao, Z.W., Ma, J.L., 2004. SHRIMP zircon geochronology and Nd–Sr isotopic geochemistry of the Dexing granodiorite porphyries. Acta Petrol. Sin. 20, 315–324 (In Chinese with English abstract).
Wang, G.G., Ni, P., Zhao, K.D., Liu, J.R., Xie, G.A., Xu, J.H., Zhang, Z.H., 2011. Comparison of fluid inclusions in coexisting sphalerite and quartz from Yinshan deposit, Dexing, Northeast Jiangxi Province. Acta Petrol. Sin. 27, 1387–1397 (In Chinese with English abstract).
Wang, C.Y., Li, X.F., Xiao, R., Bai, Y.P., Yang, F., Mao, W., Jiang, S.K., 2012. Elements mobilization of mineralized porphyry rocks during hydrothermal alteration at Zhushahong porphyry copper deposit, Dexing district, South China. Acta Petrol. Sin. 28, 3869–3886 (In Chinese with English abstract).
Wang, G.G., Ni, P., Wang, R.C., Zhao, K.D., Chen, H., Ding, J.Y., Zhao, C., Cai, Y.T., 2013. Geological, fluid inclusion and isotopic studies of the Yinshan Cu–Au–Pb–Zn–Ag deposit, South China: implications for ore genesis and exploration. J. Asian Earth Sci. 74, 343–360.
Wang, Z.L., Yang, L.Q., Guo, L.N., Marsh, E., Wang, J.P., Liu, Y., Zhang, C., Li, R.H., Zhang, L., Zheng, X.L., Zhao, R.X., 2015. Fluid immiscibility and gold deposition in the Xincheng deposit, Jiaodong Peninsula, China: a fluid inclusion study. Ore Geol. Rev. 65, 701–717.
Wu, F.Y., Ge, W.C., Sun, D.Y., Guo, C.L., 2003. Discussions on the lithospheric thinning in eastern China. Earth Sci. Front. 10 (3), 51–60 (in Chinese with English abstract).
Wysoczanski, R.J., Handler, M.R., Schipper, C.I., Leybourne, M.I., Creech, J., Rotella, M.D., Nichols, A.R.L., Wilson, C.J.N., Stewart, R.B., 2012. The tectonomagmatic source of ore metals and volatile elements in the Southern Kermadec Arc. Econ. Geol. 107, 1539–1556.
Xiao, Q.H., Li, Y., Feng, Y.F., Qiu, R.Z., Zhang, Y., 2010. A preliminary study of the relationship between Mesozoic lithosphere evolution in eastern China and the subduction of the Pacific plate. Geol. China 37, 1092–1101 (In Chinese with English abstract).
Xie, Y.L., Tang, Y.W., Li, Y.X., Li, Y., Liu, B.S., Qiu, L.M., Zhang, X.X., Jiang, Y.C., 2012. Magmatic intrusive series and their implication for the ore prospecting in Anji exploration area, Zhejiang province. Acta Petrol. Sin. 28, 3334–3346 (In Chinese with English abstract).
Xu, Z.Z., Zhang, H.T., Jiang, Y., 1981. Study on the conditions of structure to control the ore in Jiande copper deposit. J. Chengdu Inst. Geol. 2, 6–17 (In Chinese with English abstract).
Yang, M.G., Mei, Y.W., 1997. Characteristics of geology and metallization in the Qinzhou-Hangzhou paleoplate juncture. Geol. Miner. Resour. South China 52–59 (In Chinese with English abstract).
Yang, K.H., Scott, S.D., 2002. Magmatic degassing of volatiles and ore metals into a hydrothermal system on the modern sea floor of the eastern Manus back-arc basin, western Pacific. Econ. Geol. 97, 1079–1100.
Yang, K.H., Scott, S.D., 2006. Magmatic fluids as a source of metals in seafloor hydrothermal systems. Geophys. Monogr. Ser. 166, 163–184.
Yang, M.G., Huang, S.B., Lou, F.S., Tang, W.X., Mao, S.B., 2009. Lithospheric structure and large-scale metallogenic process in Southeast China continental area. Geol. China 36, 528–543 (In Chinese with English summary).
Yu, Y.P., 2010. Geological characteristics of deposit and distribution law of main ore elements in Songkengwu ore block of Zhejiang Jiande copper mine. Miner. Resour. Geol. 24, 407–413 (In Chinese with English abstract).
Zartman, R.E., Doe, B.R., 1981. Plumbotectonics—the model. Tectonophysics 75, 135–162.
Zeng, Q.D., Wang, Y.B., Zhang, S., Liu, J.M., Qin, K.Z., Yang, J.H., Sun, W.D., Qu, W.J., 2013. U–Pb and Re–Os geochronology of the Tongcun molybdenum deposit and Zhilingtou

gold–silver deposit in Zhejiang province, southeast China, and its geological implications. Resour. Geol. 63, 99–109.
Zhang, J.J., Mei, Y.P., Wang, D.H., Li, H.Q., 2008. Isochronology study on the Xianglushan scheelite deposit in north Jiangxi province and its geological significance. Acta Geol. Sin. 82 (7), 927–931 (In Chinese with English abstract).
Zhang, J.F., Gong, R.J., Xie, H.S., Xu, X.M., 2013. Ore deposit types and petrogenesis and metallogenesis in Lizhu Region, Northwestern Zhejiang Province. Acta Geol. Sin. (Engl. Ed.) 87 (z1), 824.
Zhen, J.H., 2003. Study and application of geological structure of ore-formation in Jiande copper mine. Express Inf. Min. Ind. 7–8 (In Chinese with English abstract).
Zheng, Y.F., Zhao, Z.F., Chen, Y.X., 2013. Continental subduction channel processes: plate interface interaction during continental collision. Chin. Sci. Bull. 58, 4371–4377.
Zhou, J.Y., Huang, J.J., Yu, Z.C., 1983. Research on the.ore control characteristics, ore solution migration and metallogenic prognosis at the Jiande copper ore deposit, Zhejiang province. J. Chengdu Inst. Geol. 10, 1–22 (In Chinese with English abstract).
Zhou, X.M., Sun, T., Shen, W.Z., Shu, L.S., Niu, Y.L., 2006. Petrogenesis of Mesozoic granitoids and volcanic rocks in South China: a response to tectonic evolution. Episodes 29, 26–33.
Zhou, Q., Jiang, Y.H., Zhang, H.H., Liao, S.Y., Jin, G.D., Zhao, P., Jia, R.Y., Liu, Z., 2013a. Mantle origin of the Dexing porphyry copper deposit, SE China. Int. Geol. Rev. 55, 337–349.
Zhou, L.Y., Wu, G.M., Liu, R., Qian, J.F., Xu, F.Q., 2013b. Geochemistry and genesis of the Yinshan silver polymetallic deposit in Chun'an county, Zhejiang province. Geol. Sci. Technol. Inf. 32, 112–117 (In Chinese with English abstract).